Validation and Biomechanical Measurements using a Novel Inertial Measurement Unit

Sigurbjörg Jónsdóttir

Thesis of 30 ECTS credits
Master of Science in Biomedical Engineering

June 2014

Validation and Biomechanical Measurements using a Novel Inertial Measurement Unit

Sigurbjörg Jónsdóttir

Thesis of 30 ECTS credits submitted to the School of Science and Engineering
at Reykjavík University in partial fulfillment
of the requirements for the degree of
Master of Science in Biomedical Engineering.

June 2014

Supervisor(s):

Magnús Kjartan Gíslason, Supervisor
Assistant Professor, Reykjavík University, Iceland

Examiner(s):

Ólafur Haukur Sverrisson, Examiner
Engineer, Össur hf, Iceland

Abstract

An Inertial Measurement Unit (IMU) is an important sensor that measures the orientation of the object it is attached to. To be able to utilize and validate the IMU sensor correctly, an understanding of the data from each sensor in the IMU, accelerometer, gyroscope and magnetometer is essential to be able to adjust the data into usable and comparable information to other methods. In the literature Kalman filter is the most commonly used filter to fuse the data from the sensors in the IMU together but since it is complicated to implement, another filter was chosen which is easier to implement, the efficient orientation filter for inertial/magnetic sensor arrays. An experiment was done twice on 10 subjects where the Kine IMU sensor was first attached to a subject's hip and then moved and attached right above the subject's knee. The subjects jumped in place on top of a force plate where the jump was captured on video. Data from video analysis and force plate were used to compare the data from the Kine IMU sensor. All three datasets had very similar tracks but the peaks had different amplitudes. This results indicate that the data from the Kine IMU sensor is accurate and, following proposed development listed in this thesis, could become a very user friendly IMU sensor.

Keywords: IMU, accelerometer, gyroscope, magnetometer, orientation

Úrdráttur

Tregðunemi (IMU) er mikilvægur nemi sem mælir stefnu hlutar sem hann er tengdur við. Til að geta sannprófað og nýtt tregðunemann á réttan máta er nauðsynlegt að skilja gögnin frá hverjum mæli í tregðunemanum, hröðunarmælinum, hornhraðamælinum og segulsviðsmælinum, svo hægt sé að breyta gögnunum til að nýta þau við rannsóknir og til að bera þau saman við gögn frá öðrum sambærilegum mælum. Í fræðigreinum er Kalman sía mest notaða sían til að samtengja gögnin frá mælunum í tregðunemanum, en þar sem flókið er að setja upp Kalman síuna þá var önnur notendavænni sía valin, skilvirk stefnusía fyrir tregðu/seguls nema vektora (efficient orientation filter for inertial/magnetic sensor arrays). Tilraun var framkvæmd tvisvar á 10 einstaklingum þar sem Kine tregðuneminn var fyrst festur við mjöðm og síðar var neminn færður og festur rétt fyrir ofan hnéð á hverjum einstakling. Einstaklingurinn stökk beint upp, ofaná kraftplötu og myndavél tók upp stökkið. Gögn frá myndbandsgreiningunni og kraftplötunni voru notuð til að bera saman við gögn frá tregðunemanum. Ferlarnir voru svipaðir í öllum þremur gagnasettunum en topparnir voru mis háir. Þetta leiðir til kynna að gögnin frá Kine tregðunemanum séu rétt. Ef þeim breytingum á nemanum sem lagðar eru til í þessari ritgerð er fylgt eftir, þá gæti þetta orðið mjög notendavænn tregðunemi.

Lykilorð: Tregðunemi, hröðunarnemi, snúðspóla, segulsviðsnemi, stefna

Validation and Biomechanical Measurements using a Novel Inertial Measurement Unit

Sigurbjörg Jónsdóttir

30 ECTS thesis submitted to the School of Science and Engineering
at Reykjavík University in partial fulfillment
of the requirements for the degree of
Master of Science in Biomedical Engineering.

June 2014

Student:

_____

Sigurbjörg Jónsdóttir

Supervisor(s):

_____

Magnús Kjartan Gíslason

Examiner:

_____

Ólafur Haukur Sverrisson

Acknowledgment

I would like to thank my supervisor Dr. Magnús Kjartan Gíslason for the useful comments, remarks and for the help he has provided throughout this project.

Also I would like to thank Ásmundur Eiríksson and Baldur Þorgilsson at Kine for all their input in this project, quick problem solving and their willingness to assist at any time.

Furthermore I would like to thank Nils Óskar Nilsson for helping me with the set-up of my research and Torfi Þórhallsson for helping me analyze the data.

Finally I would like to thank my boyfriend Ruben Severino for putting up with me these last couple of months and my family for all of their love and support during this time. Specially Snæbrá Krista Jónsdóttir for proofreading this thesis and Gunnþóra Snæþórsdóttir for proofreading the Icelandic part.

Contents

Abstract i
Úrdráttur ii
Acknowledgment iv
List of Tables vii
List of Figures viii
1. Introduction 1
1.1. Background 1
1.2. Goals of the Project and Motivation 2
1.3. Structure of this Thesis 2
2. Literature Review 3
2.1. Introduction 3
2.2. Accelerometers 3
2.2.1 A Three-Axial Accelerometer 5
2.3 Gyroscope 6
2.3.1. Three-Axial Gyroscope 7
2.4 Magnetometer 7
2.5 IMU 8
2.5.1. Accelerometer in IMU 9
2.5.2. Gyroscope and Magnetometer in IMU 10
2.6. Kalman Filter 10
2.7. An efficient Orientation Filter for Inertial/Magnetic Sensor Arrays 12
2.7.1. Quaternion Representation 12
2.7.2. Euler Angles 13
2.7.3. About the IMU and AHRS Algorithm 14
2.8. Usage of IMU in Bioengineering 16
2.9. Technical Description of the Kine IMU Sensor 19
2.9.1 Introduction 19
2.9.2. Appearance 19
2.9.3. The Gyroscope 20
2.9.4. The Three-Axis Accelerometer and Three-Axis Magnetometer 22
2.9.5. The Users Program 24

3. Materials and Methods 26
3.1. Scaling and Examination of the IMU Data 26
3.2. Recruitment of Subjects for the Experiment 26
3.3. Experimental Set-up 27
3.4. Framework for Data Analysis Technique 28
4. Results 28
4.1. Scaling and Examination of the IMU Data 28
4.2. Biomechanical Experiment 32
4.2.1. Other Data from the Experiment 37
5. Discussions 40
5.1. The Experiment 40
5.2. Errors Estimating 41
5.2.1. Errors because of the Kine IMU Sensor 41
5.2.2. Errors because of the Video Analysis 41
5.2.3. Errors because of the Force Plate 41
5.3. Future Work 41
5.3.1. Making the Connection from the Kine IMU to the Computer easier 41
5.3.2. Making the Sensor into one Unit 42
5.3.3. Making it Cordless 42
5.3.4. Making the Sensor more Stable 43
6. Conclusion 43
References 44
Appendix A - Matlab Code 46

List of Tables

Table 1: The trade-offs between the sensor types, modified from [16] 8
Table 2: Variables that are in the Kalman filter [20] 10
Table 3: Similar experiments that others have done. Made from information from [2][3][24][25][26][27] 18
Table 4: The main mechanical characteristics of the gyroscope [28] 21
Table 5: The main mechanical characteristics of the accelerometer and magnetometer [29] 23

List of Figures

Figure 1: A schematic diagram of a strain-gauge accelerometer [12] 4
Figure 2: A typical design of a three-axial accelerometer [6] 5
Figure 3: A structure of a regular gyroscope [10] 6
Figure 4: Roll, pitch and yaw angles 9
Figure 5: Schematic diagram of the algorithm for the Kalman filter [20] 11
Figure 6: The orientation of frame B is achieved from alignment with frame A by a rotation of angle θ around the axis $\boldsymbol{Ar}$ [5] 13
Figure 7: The aerospace Euler angle-axes sequence [21] 13
Figure 8: A block diagram that represent the complete orientation filter for a MARG implementation that includes magnetic distortion (Group 1) and gyroscope drift (Group 2) compensation [5] 14
Figure 9: The image to the left is a close up of the sensor connected to the elastic belt, the image on the right shows both units side to side 20
Figure 10: The size and direction of detectable angular rates of the gyroscope L3G4200D [28] 21
Figure 11: A block diagram of the gyroscope L3G4200D. Adapted from [28] 22
Figure 12: The size and the directions of the detectable magnetic fields and accelerations in the sensor [29] 23
Figure 13: A block diagram of the accelerator and magnetometer LSM303DLH. Adapted from [29] 24
Figure 14: The program used to retrieve the data from the Kine IMU sensor 25
Figure 15: A picture from the experiment, to the left the IMU sensor is attached to the hip, to the right the IMU sensor is attached right above the knee 27
Figure 16: Turning the Kine IMU sensor around its x-axis 29
Figure 17: Turning the Kine IMU sensor around its y-axis 29
Figure 18: Turning the Kine IMU sensor around its z-axis 30
Figure 19: Kine IMU sensor lays still on table for about 30 minutes 31
Figure 20: Subject 4, sensor on hip. It can be seen that the gyroscope is not working as it should 32
Figure 21: Comparison of different methods of measuring acceleration and angle of the Kine IMU sensor, on subject 1, where the sensor was put right above the knee 33

Figure 22: Comparison of different methods of measuring acceleration and angle of the Kine IMU sensor, on subject 3, where the sensor was put on the hip 34
Figure 23: Comparison of different methods of measuring acceleration and angle of the Kine IMU sensor, on subject 3, where the sensor was put right above the knee 34
Figure 24: Comparison of different methods of measuring acceleration and angle of the Kine IMU sensor, on subject 7, where the sensor was put on the hip 35
Figure 25: Comparison of different methods of measuring acceleration and angle of the Kine IMU sensor, on subject 8, where the sensor was put on the hip 35
Figure 26: Comparison of different methods of measuring acceleration and angle of the Kine IMU sensor, on subject 8, where the sensor was put right above the knee 36
Figure 27: Comparison of different methods of measuring acceleration and angle of the Kine IMU sensor, on subject 9, where the sensor was put on the hip 36
Figure 28: Comparison of different methods of measuring acceleration and angle of the Kine IMU sensor, on subject 9, where the sensor was put right above the knee 37
Figure 29: A comparison of the highest values of the acceleration data from the each subject ... 37
Figure 30: Percentage different between the data from the Kine IMU sensor to the video analysis. Dataset from subject 9, sensor on hip 38
Figure 31: The Euler angles and the angle from the video analysis for subject 9, sensor on hip . 39
Figure 32: The movement of the Kine IMU sensor during the video analysis, on subject 9, sensor on hip 40

1. Introduction

1.1. Background

An accuracy in measuring the orientation of an object is important in many fields, such as human motion analysis, aerospace, navigation, machine interaction and robotics [1]. There are currently many fundamental tracking technologies, for example electromagnetic tracking, inertial/magnetic tracing mechanical tracking, optical tracking and acoustic tracing [2].

The technologies of tracking human motion have started to be increasingly used in many applications such as sports, health monitoring, rehabilitation, interactive gaming, music training and augmented reality [3].

IMU (Inertial Measurement Unit) is a sensor that consist of gyroscopes and accelerometers, and in recent years, a magnetometer as well. A better definition of the sensor used in this thesis is a MARG (Magnetic, Angular Rate, and Gravity) sensor, which is called a hybrid IMU, because in its definition the sensor always includes magnetometers. In this thesis this sensor will be called an IMU. In both IMU and MARG an orientation estimation algorithm is a fundamental component. It is required to fuse together the data from each sensor into a single estimate of orientation [1].

Numerous methods have been tried to fuse these different sensor data together. In the beginning it was assumed that the gravity would not affect the acceleration, which gave unacceptable errors in recordings of human motion. Then a popular applied method was to estimate the orientation by integrating the angular rate which was measured with rate gyroscopes. However an error measured in the angular rate would result in an increasing inaccuracy in the estimated orientation, by integrating the angular rate, the error was integrated as well and drift errors were made [2][4]. To compensate the drift of the gyroscope the accelerometer can be used for the drift in the horizontal plane, while the magnetometer can solve the drift problem in vertical axis [4]. An improved algorithm was needed to connect these signals and in recent years the Kalman filter has become the most used algorithm for orientation [1].

Kalman filter has shown itself to be accurate and effective, nevertheless it has number of disadvantages, the main being that it can be quite complicated to implement. In 2010 Madgwick published an algorithm, called an efficient orientation filter for inertial and inertial/magnetic sensor

arrays, which is easier to implement and is supposed to have the same accuracy and effectiveness as the Kalman filter [1][5]. What makes the efficient orientation filter for inertial and inertial/magnetic sensor arrays easier to implement than the Kalman filter is that the algorithm for the orientation filter has been pre coded for general use, the only parameters that this algorithm needs are the data files in correct format (which is discussed in chapter 4.1.) from the accelerometer, gyroscope and magnetometer, and an all mean zero gyroscope measurement error. When using Kalman filter the algorithm needs to be programed and doing that is challenging since there are many parameters that go into making the algorithm.

1.2. Goals of the Project and Motivation

The Kine IMU sensor is a prototype that Kine is working on. The aim of this thesis is to validate the data from this sensor. This was done by adjusting the data from the Kine IMU sensor to make it possible to compare it to data from a video analysis and a force plate. Since this sensor is a prototype, an evaluation of the sensor was also performed.

The motivation behind this experiment was to become confident in that the Kine IMU sensor is producing accurate data as well finding a method that could transforms the data into readable information.

1.3. Structure of this Thesis

Chapter 1: Introduction

In this chapter the reader is provided with a background information about IMU sensors and what methods have been used to fuse the data together from these three different sensors. The focus of the research is discussed as are the goals and motivation of this thesis.

Chapter 2: Literature Review

In this chapter a literature review is done for all three sensors accelerometer, gyroscope and magnetometer and how they work together to create an IMU sensor. Similar studies are presented. Also a short discussion is done on the Kalman filter since it is currently the most commonly used method to fuse the data together from IMU sensors. A review is done for the efficient orientation filter for inertial/magnetic sensor arrays, which is an algorithm based on similar theory as the

Kalman filter and an explanation why it was decided to use this filter over Kalman filter. In the end a technical description of the Kine IMU sensor that was used for this experiment, is presented.

Chapter 3: Materials and Methods

In this chapter is a description on how the Kine IMU sensor was scaled and examined. A brief discussion is had on the subjects in this research and an explanation on how the set-up was for the experiment, together with a framework for the data analysis.

Chapters 4, 5 and 6: Results, Discussion and Conclusion

In chapter 4 a report of the results from the scaling and the biomechanical experiment are presented. In the following chapter a discussion of the experiment is done as well as an error estimating of the data from the Kine IMU sensor, video analysis and force plate. In the end of chapter 5 a detailed overview is done for future work that must happen before the Kine IMU sensor can be sold commercially. In the last chapter a conclusion for this thesis is presented.

2. Literature Review

2.1. Introduction

Three-axial accelerometers are able to acquire and estimate various kinematics values, of any body segment it is attached to, such as velocity and displacement. These sensors on their own have high integration drift errors. To overcome these errors an integration of three-axis gyroscope and three-axis magnetometer have been added to the accelerometer unit to make an inertial measurement unit (IMU). A sensor fusion algorithm, that connects the sensors data together, has also been integrated in the IMU system to provide necessary kinematics parameters [6].

Kine is a company in Iceland that focuses on medical engineering. This company has developed a small surface electromyography (sEMG) unit, which is used in their Kine Measurement System, and this system produced sEMG data. This Kine IMU sensor which is used in this experiment is the next generation sensor for the Kine Measurement System [7][8][9].

2.2. Accelerometers

Accelerometer measures the acceleration that it is subjected to, including gravity which needs to be subtracted from the measured acceleration [10]. Most accelerometers are force transducers that measure the reaction forces that are associated with a given acceleration. Force transducers

measure the force, which is usually a piezoresistive type, piezoelectric or a strain gauge [11][12]. The equation that the accelerometer follows is $F=ma$, where F is the force that the segment (a) with mass (m) produces, because of the acceleration [11]. Standard accelerometers can only measure one component of the acceleration vector, so to get the acceleration in all three-dimensions a three-axis accelerometer is needed [13].

Modern accelerometers are usually micro electromechanical systems (MEMS), which consist of a cantilever beam with a proof mass. These accelerometers that are sold commercially are piezeresistive, piezoelectric, and capacitive components that convert the mechanical and/or position to an electrical signal [10]. Piezoelectric effect happens when a certain crystal cause voltage when they are mechanically stressed and compressed. Piezoelectric accelerometers do not have a true static response which means that they should not be used when recording slow movements or periods of inactivity, still they usually have higher frequency responses than strain gauge accelerometers [12].

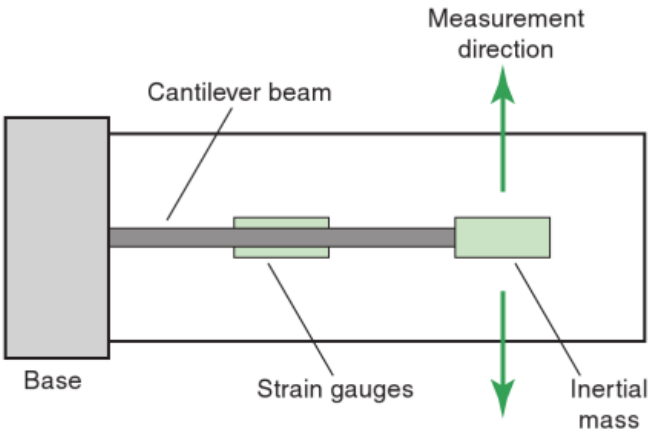

Figure 1: A schematic diagram of a strain-gauge accelerometer [12]

Figure 1 shows the inner workings of a strain gauge accelerometer. The bending of the beam is measured with small stain gauges that are attached to a cantilevered beam. The inertial mass at its free end is what causes the beam to bend in proportion to the acceleration. These accelerometers are easily damaged so it is important to handle them with care [12].

A voltage signal is produced when a mass, which is known and is constant, accelerates against a force transducer, this signal is in proportion to the force and acceleration. The data collected shows which way the acceleration is with the sign before the signal. If the acceleration

is toward the transducer then the signal is positive, the sign is reversed for acceleration away from the transducer [11].

2.2.1 A Three-Axial Accelerometer

A three-axial accelerometer is a 3D transducer with three individual accelerometers that are mounted at right angles to each other on a rigid body, where each one of them is reacting to the orthogonal component that acts on its axis and with their sensitive axes coinciding with the principal axes of inertia of the moving body [11][14].

The output of the three-axial accelerometer in the body-fixed frame (B) is given by the following measurement vector [14]:

$$f = M_N^B(q)(a - G) + d_f \tag{1}$$

Where G = $[0\ 0\ g]^T$ and a=$[a_x\ a_y\ a_z]^T$ represent the gravity vector and the dynamic body acceleration of the rigid body, given inside the Earth-fixed frame (*N*). d_f is the noise vector that is assumed to be independent, white, and Gaussian. $M_N^B\ (q)$ is the rotation matrix that reflects the transition between frames (*N*) and (*B*). An example of a rotation matrix in terms of quaternion can be see below [14]. An explanation of quaternion can be seen in chapter 2.7.1..

$$M_N^B\ (q) = \begin{bmatrix} 2(q_0^2 + q_1^2) - 1 & 2(q_1q_2 + q_0q_3) & 2(q_1q_3 - q_0q_2) \\ 2(q_1q_2 - q_0q_3) & 2(q_0^2 + q_2^2) - 1 & 2(q_0q_1 + q_2q_3) \\ 2(q_0q_2 + q_1q_3) & 2(q_2q_3 - q_0q_1) & 2(q_0^2 + q_3^2) - 1 \end{bmatrix} \tag{2}$$

Figure 2 shows a typical design for a three-axial accelerometer, it suspends a cubic mass by springs on all of the six sides. The 3D displacements of the mass with respect to the housing are measured by capacitance to acquire the acceleration values in all three dimensions [6].

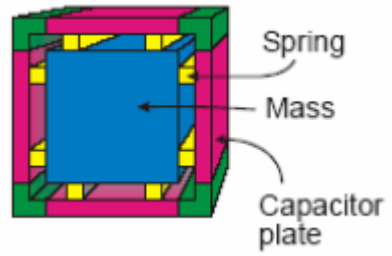

Figure 2: A typical design of a three-axial accelerometer [6]

2.3 Gyroscope

Gyroscope is a device that measures changes in objects orientation around a particular axis. [15][16]. When gyroscope is used as a sensor then it measures the angular velocity of a reference attached to the sensor [14].

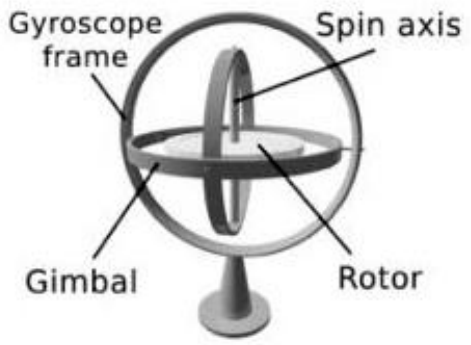

Figure 3: A structure of a regular gyroscope [10]

A definition of a gyroscope is that it is a rotating mechanism that is in the form of a universally mounted spinning wheel that offers resistance of movement in any direction. It utilizes the angular momentum of a spinning mass so it can sense angular motion of its base in one or two axes orthogonal to the spin axis, this is also called a gyro [17].

The principle of the conservation of angular momentum is what gyroscopes are based on. The angular momentum has the tendency of a rotating object to keep rotating around the same axes of rotation at the same angular speed in the absence of an external torque, as can be seen with Equation (3) [15]:

$$\boldsymbol{L} = \boldsymbol{I} \times \omega \tag{3}$$

Where $\boldsymbol{L}$ is the angular momentum of an object with moment of inertia $\boldsymbol{I}$ rotating at angular speed ω [15].

Gyroscopes are very complex objects since they move in unusual ways [7]. The rotating frame of reference is not the inertial frame, and by exploiting the rotating frames of reference physical properties a measurement can be made to estimate the relative rotation [15]. Gyroscopes are used in various applications, from sensing either the angle turned through by a vehicle or structure or, which is more common, its angular rate of turn about any defined axis [17]. There are

three basic types of gyroscopes: vibrating mass gyroscope, ring laser gyroscope and spinning rotor gyroscope. The most suitable gyroscope is the vibrating mass gyroscope, because of its portable applications due to its weight, size, power consumption and cost [6].

An example of roles that a gyroscope might have is [17]:

- Autopilot feedback
- Navigation
- Flight path stabilization
- Sensor or platform stabilization

In this thesis the focus is on how the gyroscope is being used as a sensor so examples on devises that uses gyroscopes as a sensor are [17]:

- Vibratory gyroscopes
- Electrostatic gyroscopes (ESGs)
- Rate transducers, that also include magneto – hydrodynamic and mercury sphere sensors
- Nuclear magnetic resonance (NMR) gyroscopes
- Optical rate sensors

2.3.1. Three-Axial Gyroscope

The output from the three-axial gyroscope can be given with the measurement vector [14]:

$$\omega_G = \omega + b + \delta_G \tag{4}$$

Where ω is the actual angle velocity, b is the gyro bias error and δ_G is the gyro random drift.

2.4 Magnetometer

A magnetometer is a device that measures the intensity and direction of a magnetic field, especially the Earth's magnetic field. The output from the three-axis magnetometer in the body-fixed frame (B) is given by the following measurement vector [14]:

$$h = M_N^B(q)m + d_h \tag{5}$$

Where m is the magnetic field expressed in the Earth-fixed frame (N) by

$$m = [m_x\ 0\ m_z]^T = [\|m\|\cos(\mathrm{I})\ \ 0\ \ \|m\|\sin(I)]^T \tag{6}$$

δ_h is a white Gaussian noise, and $M_N^B(q)$ is the rotation matrix [14].

The magnetometer has been indicated in some studies to be sensitive to ferromagnetic materials, like iron, and other metal magnetic materials, this results in distortion in the orientation estimate [6].

2.5 IMU

Inertial Measurement Unit combines the technology of three accelerometers, three gyroscopes and three magnetometers. This system has recently begun to be used in intelligent gait humanoids, a usage of miniature body-mounted sensors has been considered as an alternative method to collect the kinematics parameters of the human movement [6][16]. By having three-axial accelerometers and gyroscopes, it is possible to estimate where the object is heading and how its motion changes in all three directions [17]. The reason behind adding a three-axis magnetometer is to subtract the gravity field signal from the acceleration signal and it allows for better performance in the dynamic orientation calculation [6] [10]. Accelerometer measures the linear acceleration of the object, the gyroscope measure the angular rate that the object is under, and the magnetometer is used as an horizontal reference when calculating the rotational angle [16].

Each sensor has got his strengths and weaknesses that are important to know and understand when using the IMU, these trade-offs can be seen in Table 1.

Table 1: The trade-offs between the sensor types, modified from [16]

Sensor	Strengths	Weaknesses
Accelerometer	Very linear Needs very little power Inexpensive Has low noise	Measures the difference of acceleration and gravity. Very important to separate them.
Gyroscope	Fairly independent of linear acceleration Is possible to use to “gyro-compensate” the magnetometer	Uses a lot of power Has a long start up time Zero rate offset drift over time
Magnetometer	Can orient itself with regard to “north” Insensitive to linear acceleration	Subject to magnetic interference Not constant with location within office environments

Small offset on the gyroscope signal will give a large integration errors, to try and minimize this error an application of Kalman filter that fuses together the signals from the three-axial accelerometer and three-axial gyroscope. Another way to minimize the error is by applying auto-resetting and auto-nulling the algorithm [6].

Recent advantages in MEMS technologies have made the IMU into a small size, light weight, low cost and low power consumption measurement unit. That has made it possible to use the IMU in a variety of applications, ranging from measurements of human movements to the balancing system in a Segway personal transporter, previously it was mainly used in expensive research and work, for example in aerospace research or form of military application [6][10].

2.5.1. Accelerometer in IMU

The accelerometer measures the sum of gravity and all inertial forces. Because of this the accelerometer can be used as inclinometers [18]:

$$\theta_A = \arcsin(A_x/g) \tag{7}$$

$$\phi_A = \arcsin(A_y, A_z) \tag{8}$$

Where, θ_A: is the pitch angle by the data of accelerometer

ϕ_A: is the roll angle by the data of accelerometer

A_x, A_y, A_z: is the output of accelerometer

g: is the gravity

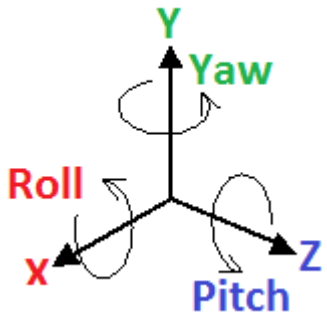

Figure 4: Roll, pitch and yaw angles

Figure 4 shows how the roll, pitch and yaw angles are presented. Roll is movement around x-axis, pitch is movement around z-axis, and yaw is movement around y-axis.

2.5.2. Gyroscope and Magnetometer in IMU

As previously mentioned, the gyroscope measure the rotational velocity and in order to obtain the angle of rotation integration is needed of the sensor signal. However, carrying out the integration the smallest constant bias can result in error growing to infinity. The biggest error in rate gyro is the drift. The Kalman filter is used in effort to minimize the drift error. Therefore the following analysis is carried out [18]:

$$\bar{\omega} = \omega_m - \omega_e \tag{9}$$

Where, $\bar{\omega}$: is the biased compensated gyro measurement

ω_m: is the output of the gyroscope

ω_e: is the estimated bias drift by Kalman filter

The three-axis magnetometer is used to correct the gyro-derived heading [19].

2.6. Kalman Filter

The Kalman filter is better considered as a computer algorithm rather than a filter. In Figure 5 the whole computational process for the Kalman filter is put out in a schematic diagram. The procedure is divided into four stages, there are some cases with abbreviated procedure or different style of beginning but the essence of the algorithm remains the same [20].

Table 2: Variables that are in the Kalman filter [20]

External input	z_k (measurement)
Final output	$\hat{x}_k$ (estimate)
System model	A, H, Q, R
For internal computation	$\hat{x}_k^-$, P_k^-, P_k, K_k

Table 2 shows the variables that are in the Kalman filter. The "external input" is the data that is measured and then put in the filter. The "final output" is the estimate that the Kalman filter computes. The "system model" variables should be set before implementing the Kalman filter, these values are set by the user according to the characteristics of the system and purpose of Kalman filter. The "internal computation" variables are calculated in the Kalman filter (which can be seen in Figure 5). The subscript *k* corresponds to the Kalman filter algorithm is being executed and the subscription "-" corresponds to the predicted value [20].

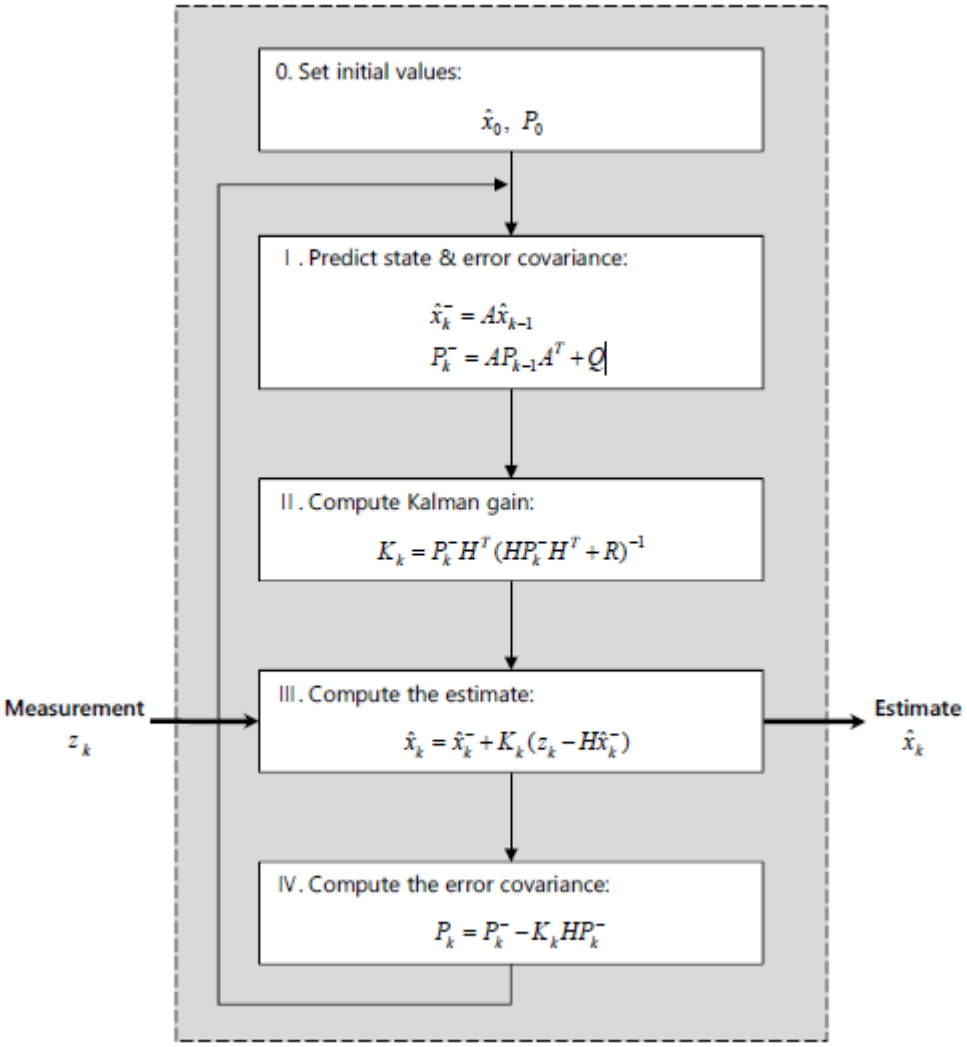

Figure 5: Schematic diagram of the algorithm for the Kalman filter [20]

As can be seen on Figure 5 the structure itself is fairly simple, it receives an input and then it returns an output. The Kalman filter goes through four stages [20].

A run through of what happens in each stage in Figure 5 is [20]:

1. The first stage is for the prediction, the variables $\hat{x}_k^-$ and P_k^-, that are used in stages II through IV, are computed in this step.
2. In stage II the Kalman gain (K_k) is computed.
3. In stage III an estimate is computed from the measurements given as input. The formula here is related to low-pass filter.
4. In stage IV the error covariance is computed. The error covariance (P_k) is a measure that indicates how accurate the estimate is.

2.7. An efficient Orientation Filter for Inertial/Magnetic Sensor Arrays

In this chapter the essentials of the orientation filter will be explained in a short summary.

2.7.1. Quaternion Representation

The first essentials is the quaternion representation, which is a four-dimensional complex number which can be used to coordinate frame in three-dimensional space or to represent the orientation of a rigid body. The rotation of angle θ around an axis ${}^A\hat{\boldsymbol{r}}$ which is defined in frame A represents the arbitrary orientation of frame *B* relative to frame *A*. In Figure 6 this can be seen where the orthogonal unit vectors $\hat{\boldsymbol{x}}_A$, $\hat{\boldsymbol{y}}_A$ and $\hat{\boldsymbol{z}}_A$, and $\hat{\boldsymbol{x}}_B$, $\hat{\boldsymbol{y}}_B$ and $\hat{\boldsymbol{z}}_B$ define the principle axes of coordinate frames *A* and *B.* In Equation 10 the quaternion description of this orientation, ${}^A_B\hat{\boldsymbol{q}}$, is defined, where r_x, r_y and r_z define the components of the unit vector ${}^A\hat{\boldsymbol{r}}$ in the *x*, *y* and *z* axes of frame *A* [5].

$$ {}^A_B\hat{\boldsymbol{q}} = [q_1\ q_2\ q_3\ q_4] = \left[cos\frac{\theta}{2}\ \ -r_x sin\frac{\theta}{2}\ \ -r_y sin\frac{\theta}{2}\ \ -r_z sin\frac{\theta}{2}\right] \tag{10} $$

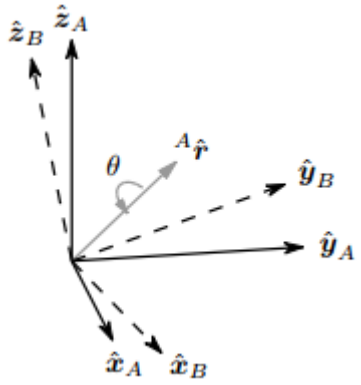

Figure 6: The orientation of frame B is achieved from alignment with frame A by a rotation of angle θ around the axis ${}^A\hat{\boldsymbol{r}}$ [5]

2.7.2. Euler Angles

The Euler angles ψ, θ and φ are in sequence which is referred to as the aerospace sequence that describes an orientation of frame *B* that is achieved by the sequential rotations from alignment with frame *A*, where ψ is around $\hat{\boldsymbol{z}}_B$, θ is around $\hat{\boldsymbol{y}}_B$ and φ is around $\hat{\boldsymbol{x}}_B$, which can be seen on Figure 7. Equations 11-13 represent this Euler angle of ${}^A_B\hat{\boldsymbol{q}}$ [5].

$$\psi = Atan2(2q_2q_3 - 2q_1q_4, 2q_1^2 + 2q_2^2 - 1) \tag{11}$$

$$\theta = -sin^{-1}(2q_2q_4 - 2q_1q_3) \tag{12}$$

$$\phi = Atan2(2q_3q_4 - 2q_1q_2, 2q_1^2 + 2q_4^2 - 1) \tag{13}$$

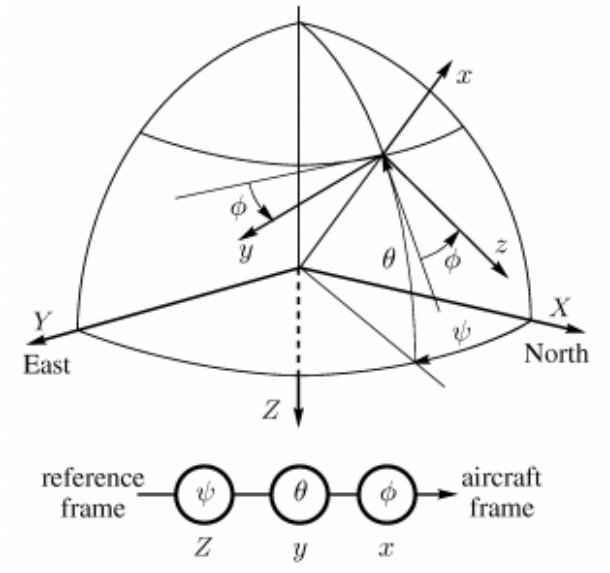

Figure 7: The aerospace Euler angle-axes sequence [21]

2.7.3. About the IMU and AHRS Algorithm

The open source IMU and AHRS algorithm that Madgwick made, from his efficient orientation filter for inertial/magnetic sensor arrays, is available in Matlab, C and C# [22]. Built in this code is a folder which contains all the quaternion and Euler calculations that are needed. Also built in is manipulation of the data set [23]:

- Normalization of the accelerometer and magnetometer measurement
- Reference direction of Earth's magnetic field
- A gradient decent algorithm corrective step
- Compute rate of change of quaternion
- Integrate to yield quaternion

This algorithm was written in United Kingdom, there the vertical component due to the earth's magnetic field is at 65° to 70° to the horizontal axis [5].

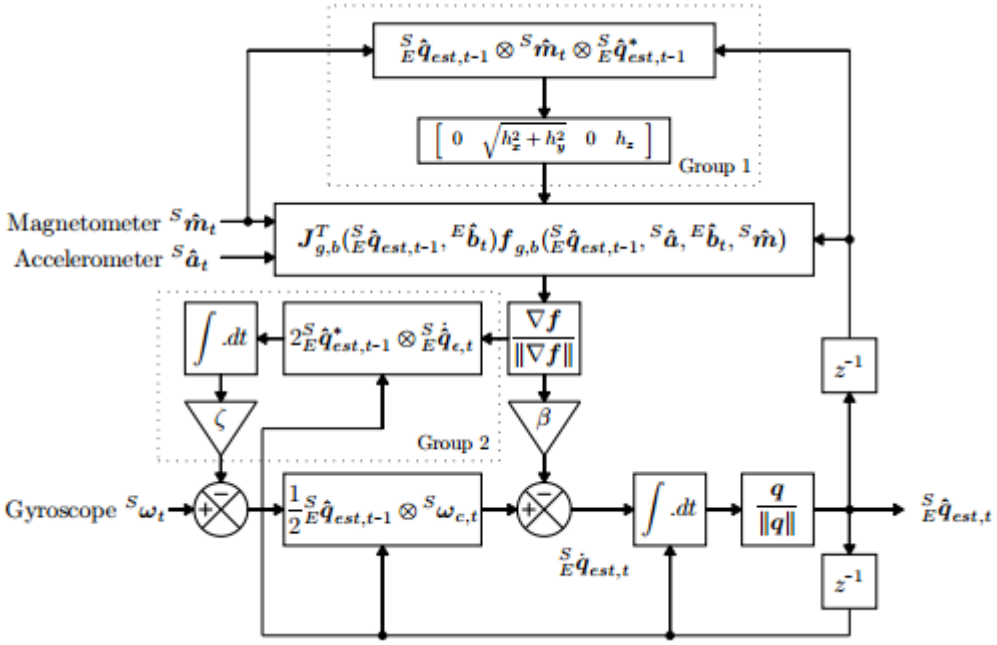

Figure 8: A block diagram that represent the complete orientation filter for a MARG implementation that includes magnetic distortion (Group 1) and gyroscope drift (Group 2) compensation [5]

Figure 8 shows a block diagram that represents the complete filter implementation for a MARG sensor array, included in it is the gyroscope bias drift compensation and magnetic distortion.

An explanation of this block diagram in steps is [5]:

1. The magnetometer signal goes through two equations in Group 1. First equation represents the measurement of the measured direction of the earth's magnetic field in the earth frame at time t, it is computed as the normalized magnetometer measurement, ${}^{S}\hat{\boldsymbol{m}}_{t}$, rotates by the estimated orientation of the sensor provided by the filter ${}_{E}^{S}\hat{\boldsymbol{q}}_{est,t-1}$. To correct the effect of the incorrect inclination of the measured direction earth's magnetic field the second equation is implemented.
2. The accelerometer and magnetometer signal go together through one equation. Because the measurement of the earth's magnetic field or gravity alone does not provide a unique orientation of the sensor this equation need to be implemented because it combines the measurements and reference direction of both fields.
3. Then the signal from step 2 goes through an equation that represents the direction of the error of ${}_{E}^{S}\hat{\boldsymbol{q}}_{est,t}$. After that the signal can either go to Group 2 or through the filter gain, β, which represents all mean zero gyroscope measurement errors, which is expressed as the magnitude of a quaternion derivative. After the signal goes through the filter gain it goes to a summary point.
4. The first equation in Group 2 gets its signal from both step 3 and from the final signal in the last measurement before this one. The first equation shows how the normalized direction of the estimated error in the rate of change of orientation, ${}_{E}^{S}\hat{\boldsymbol{q}}_{\epsilon,t}$, can be expressed as the angular error in each gyroscope axis. Then that signal is integrated and put through the filter gain, ζ, which represents the rate of convergence by removing gyroscope measurement errors which are not mean zero. This is expressed as the magnitude of a quaternion derivative. This signal then goes to a summary point.
5. The gyroscope signal goes through a summary point, picks up the signal from step 4, and goes through an equation that represent how the orientation of the earth frame relates to the sensor frame at time t.
6. Then the combined signal from step 5 and the signal from the filter gain, β, is integrated and the vector is normalized.

2.8. Usage of IMU in Bioengineering

A technique that combines the signal from a three-axis accelerometer, gyroscope and magnetometer enables 3D inter-segment joint angle measurement and could benefit variety of applications that require observation of joint angles. This technique can obtain the position and/or orientation of each segment and make a direct estimate of the joint angle. An example of measurement made by this technique is in use in drop foot correction applications or in a monitoring of a lower leg activity on persons with limited mobility that are at risk of remaining inactive for extended periods. Since this technique is not dependent on a fixed reference coordinate system it can be suitable for use in dynamic systems such as a moving vehicle. Recent advances in micro technology of the design have made it possible to integrate the motion sensing systems into clothing [3][24]. The use of accelerometers in human joint kinematics studies have been done since 1990, but only uniaxial joint kinematics could be obtained. Then in the 2000s a simplified system was developed using data from accelerometers and gyroscopes to estimate orientation relative to an inertial frame [4].

Mayagoitia et al. performed a research on 10 males where four pairs of uniaxial accelerometers were mounted on two aluminum strips and a gyroscope was attached to the midpoint of each aluminum strip. The aluminum strips were placed on frontal, medial aspect of the shank and thigh on each subject and attached with an elasticized velcro straps. Each subject performed ten 10 s or 12 s treadmill walking trials consisting of two repetitions at five speeds (varying from 1.4 km/h to 4.6km/h). Data from the accelerometer and gyroscope were recorded at 100 Hz. A Vicon motion-measurement system was used to compare the data from the accelerometer and gyroscope to, the markers were tracked at 50 Hz. A sixth-order Butterworth low-pass filter was used with a cut-off frequency of 3 Hz. The root of the mean of the squared error (RMSE) was used for the comparison of the sensors data and Vicon results [25].

Boonstra et al. performed a research on 5 subjects where two uni-axial accelerometers and one gyroscope was put on each segment. One set of sensors were placed in a box which was attached to the waist with a neoprene belt. Two sets of sensors were placed on metal strip, one was attached to sternum and the other on the frontal side of upper leg, with double – sided tape. Each subject rose from a chair, with a height of 90° knee flexion. The subjects performed two test of rising five times. The data from the accelerometer and gyroscope were recorded at 32 Hz and then

resampled to 64 Hz. Two infrared Optotrak markers were placed on the box, and two were placed on each metal plate, the Optotrak was tracked at 64 Hz. On the accelerometer data a low-pass filter was used and RMSE was calculated for filter frequencies from 0.5 to 1.5. The gyroscope data was integrated and put through a high-pass Butterworth filter. Then the accelerometer data and gyroscope data was combined to obtain an angle. Then RMSE between the angle from the combined data and angles calculated with the Optotrak signal, were calculated for filter frequencies from 0.025 to 0.5 Hz [26].

Zhu and Zhou performed an arm motion experiment where a three-axis accelerometer, three-axis gyroscope and three-axis magnetometer were attached to subject's upper trunk, right upper arm, and right lower arm. Kalman filter was used to estimate the orientation with 20-Hz updating rate [2].

Roetenberg et al. designed a portable magnetic system that was combined with gyroscope and accelerometer sensors. The sampling frequency for all the sensors was 120 Hz. A complementary Kalman filter was also designed to fuse the data from the three different sensors together [27].

O'Donovan et al. designed and evaluated a kinematic sensor based on 3D joint angle measurement technique. The technique used a combination of sensor signals from a gyroscope, accelerometer and magnetometer. In this experiment two subjects did 13 leg exercises with two sensor attached to them. One sensor was attached to the superior surface of the foot and another was attached to the front of the lower leg. Each sensor was attached to a pad that also had three markers. The sensor signals went through a low-pass filter with a cut-off frequency of 15 Hz with a sampling frequency of 500Hz. Evart 3D motion analysis system was used to compare the data from the 3D joint angle measurement technique to, the marker data was recorded at 100 Hz. Both datasets, from the sensor and marker data, were put through a low-pass filter at 5 Hz using a second order Butterworth filter. Joint coordinate system was used to calculate the joint angle. The RMSE was used to compare the angles calculated from the sensors and the angles measured by the Evart motion analysis system [24].

Salehi et al. designed and developed a low-cost and light-weight motion capturing suit that provides a long term body motion tracking. Five IMUs were positioned on suit, one at each upper-

arm and forearm and one at the torso. Each sensor acquired data at 100 Hz. Extended Kalman filter was used to estimate the IMU orientation and kinematics [3].

Table 3: Similar experiments that others have done. Made from information from [2][3][24][25][26][27]

	MAYAGOITIA ET AL (2001)	ROBERTS ET AL (2004)	ZHU ET AL (2004)	ROETENBERG ET AL (2007)	O'DONOVAN ET AL (2007)	SALEHI ET AL (2013)
USED ACCELEROMETERS	X	X	X	X	X	X
USED GYROSCOPES	X	X	X	X	X	X
USED MAGNETOMETERS			X	X	X	X
SAMPLING FREQUENCY	100 Hz	32 Hz	20 Hz	120 Hz	100 Hz	500 Hz
METHOD USED ON THE DATA			Kalman based fusion algorithm	Kalman filter		Extended Kalman filter
LOW-PASS FILTER, CUT-OFF FREQUENCY	Butterworth, 3 Hz	Butterworth filter, 1.3 Hz			Second order Butterworth filter, 5 Hz	
HIGH – PASS FILTER		Butterworth filter				

Table 3 demonstrates how the preferred method on the data from sensors changed from using a Butterworth filter to try and get rid of unwanted data (such as noise and gyro drift) to start using various types of Kalman filter to fuse the data together, also the sampling frequency has been increasing over time.

Fong et al did a systematic review of wearable inertial motion sensors in human lower limb biomechanics studies. They studied 37 different experiments done in the years 1990 – 2010 and their main findings were as follows [4]:

- 11 used three-axis accelerometer, three-axis gyroscope and three-axis magnetometer and the first was used in 2006
- Five of the experiments used low-pass filter with cut off frequencies ranging from 15-40 Hz
- Two used Butterworth filter
- Three used Kalman filter
- Two used Savitzky-Golay filter
- The motions involved in these studies
    - 23 measured walking or/and running

    - 4 measured flexion, extension, abduction and adduction
    - 2 measured sit to stand movement
    - 1 measured land from a 5 cm fall
    - 1 measured tennis serving
- To observe the accuracies of the motion sensing system they were mostly compared with video or high speed optical motion analysis systems with reflective markers
- These materials were used to fix the motion sensors on subjects' bodies:
    - 4 used elastic straps
    - 2 used Velcro straps
    - 1 used double-side adhesive tape
    - 1 used neoprene straps
    - 5 fixed the sensors on aluminum plate before attaching on subject's bodies
    - 2 put the sensors inside plastic casing before attaching on subject's bodies

2.9. Technical Description of the Kine IMU Sensor

2.9.1 Introduction

The Kine IMU sensor is comprised of two units, one is the casing under the sensors – the measurement unit, and the other is the base unit which converts the data into readable data for the computer. There are two sensor units in the measurement IMU unit. The first unit is a three-axis digital output gyroscope and the second unit is a combination of a three-axis accelerometer and three-axis magnetometer [7]. The program used to import the data from the sensor to the computer was made by Kine and is called KMUI2 test.

2.9.2. Appearance

The size of each unit is 50mm x 25mm x 13mm. Each unit is connected with a 2m USB extension cord, the measurement unit is connected to a power source while the base unit is connected to the computer. The base unit has the antenna. Figure 9 shows the Kine IMU sensor, to the left on the figure is shown how the units were fastened to the elastic belt. To the right on the figure both units are side to side and connected to the USB cables. On the figure the coordinate system that was used in this experiment is also shown.

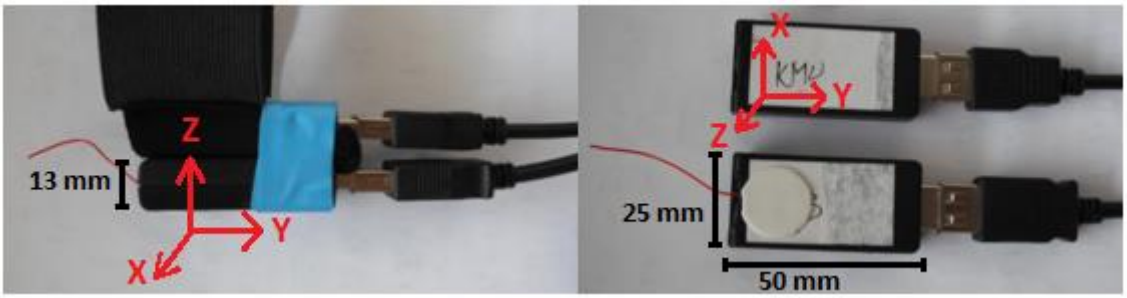

Figure 9: The image to the left is a close up of the sensor connected to the elastic belt, the image on the right shows both units side to side

2.9.3. The Gyroscope

The main features of this sensor are [28]:

- 3 selectable full scales, a 250/500/2000 degree per second (dps)
- 16 bit-rate value data output
- 8-bit temperature data output
- 2 digital output lines (interrupt and data ready)
- Integrated high- and low- pass filters that have a user selectable bandwidth
- Stability over time and over range of temperature (-40°C to + 85°C)
- Wide supply voltage: 2.4 V to 3.6 V
- Low voltage-compatible IOs (1.8 V)
- Embedded power-down and sleep mode, as well as temperature sensor
- Has high shock survivability

When the experiment was carried out the sensor was set at 2000 dps and at digital output data rate at 100 Hz. No output was taken from the temperature data and the integrated high- and low- pass filters were not used [28].

Table 4 shows the mechanical characteristics for this gyroscope, all the values are for the chosen measurement range of 2000 dps [28].

Table 4: The main mechanical characteristics of the gyroscope [28]

Parameter	Specifications	Unit
Measurement range	±2000	dps
Sensitivity	70	mdps/digit
Sensitivity change vs. temperature	±2	%
Digital zero-rate level	±75	dps
Zero-rate level change vs. temperature	±0.04	dps/°C
Self-test output change	530	dps
Rate noise density of 50 Hz	0.03	dps/sqrt(Hz)
Digital output data rate	100/200/400/800	Hz

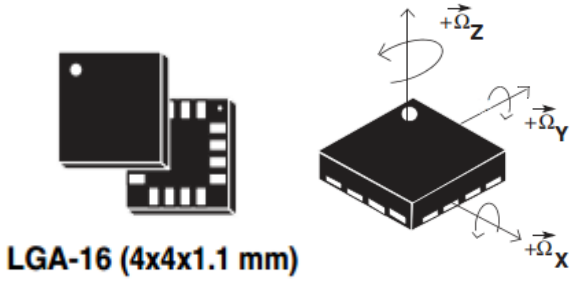

Figure 10: The size and direction of detectable angular rates of the gyroscope L3G4200D [28]

Figure 10 shows the size, appearance and the directions of the detectable angular rates is in the gyroscope [28].

This sensor is mainly used in [28]:

- Motion control with man-machine interface
- GPS navigation systems
- Gaming and virtual reality input devices
- Appliances and robotics

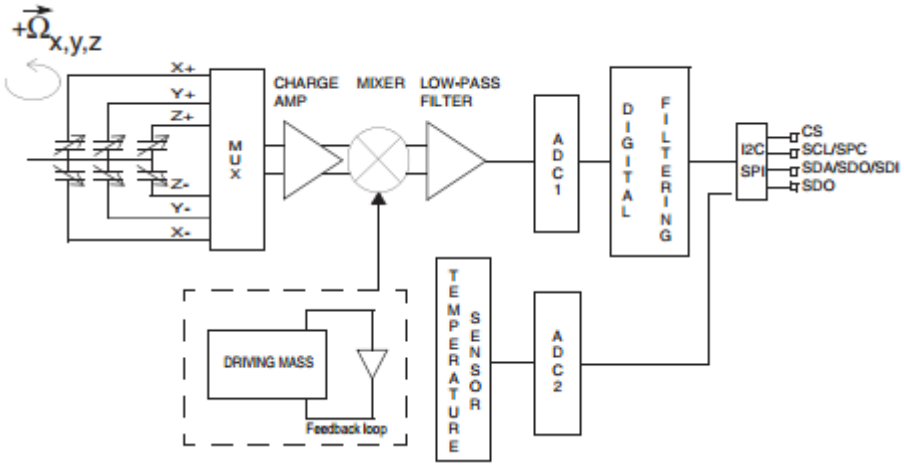

Figure 11: A block diagram of the gyroscope L3G4200D. Adapted from [28]

Figure 11 shows the block diagram of the gyroscope, the angular movement signal from each axis goes into a mixer, which is maintained by the drive circuitry in the feedback loop. Then the signals go through a low- pass filter and a digital filter [28].

2.9.4. The Three-Axis Accelerometer and Three-Axis Magnetometer

The main features of this sensor are [30]:

- Analog supply voltage: 2.5 V to 3.3 V
- Digital supply voltage IOs: 1.8 V
- Has a power-down mode
- ±1.3 to ±8.1 Gauss magnetic field full-scale
- 16-bit data out

Table 5 shows the mechanical characteristics for this accelerometer/magnetometer. All the values are for the chosen linear acceleration measurement range of ±8 g and magnetic measurement range of ±8.1 Gauss [29].

Table 5: The main mechanical characteristics of the accelerometer and magnetometer [29]

Parameter	Min	Specifications	Max	Unit
Linear acceleration measurement range		±8.0		g
Magnetic measurement range		±8.1		Gauss
Linear acceleration sensitivity	3.5	3.9	4.3	mg/digit
Magnetic gain setting for (X and Y)		230		LSB/Gauss
Magnetic gain setting for (Z)		205		LSB/Gauss
Operating temperature range		-30 to +85		°C

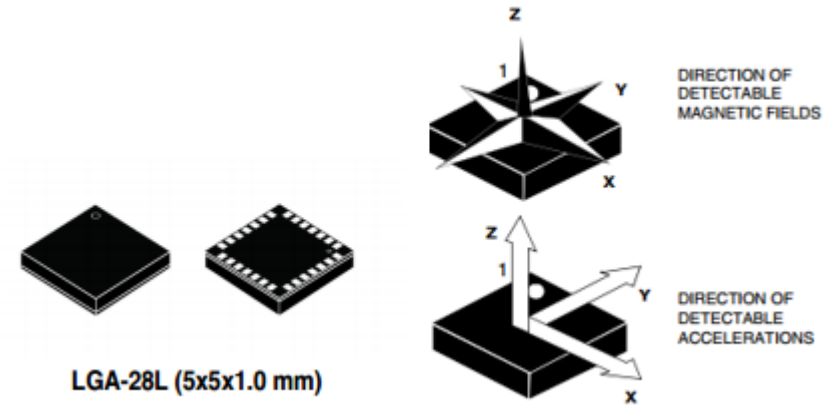

Figure 12: The size and the directions of the detectable magnetic fields and accelerations in the sensor [29]

Figure 12 shows the size, appearance and the directions of detectable magnetic fields and accelerations in this sensor [29].

What this sensor is mainly used in [29]:

- Motion-activated functions
- Map rotation
- Free-fall detection
- Compensated compassing
- Display orientation
- Position detection
- Gaming and virtual reality input devices
- Vibration monitoring and compensation

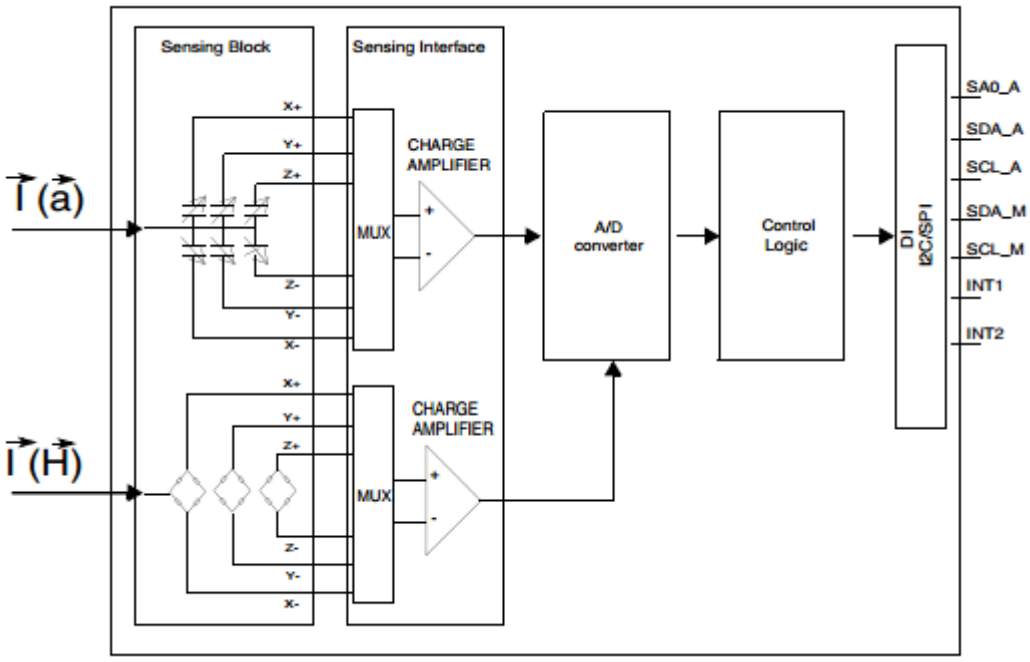

Figure 13: A block diagram of the accelerator and magnetometer LSM303DLH. Adapted from [29]

Figure 13 shows the block diagram of the accelerator and magnetometer, the accelerometer and magnetometer signal from each axis goes into the charge amplifier before going into the analog/digital converter [29].

2.9.5. The Users Program

The users program is made by Kine and is called KMUI2 test. The appearance of this program can be seen on Figure 14, on the figure the 8 steps have been labeled. After connecting the units go through the following steps:

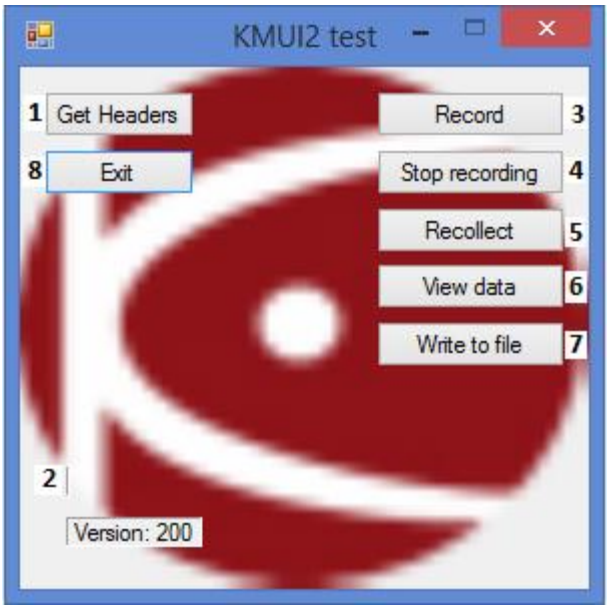

Figure 14: The program used to retrieve the data from the Kine IMU sensor

1. Press “Get Headers”.
2. After step 1 if the computer reads the sensor correctly and everything connects, then the program will show “Unit 1” in this spot. If the connections are incorrect or the computer is not reading the sensor correctly, the space will show “Unit 0”.
3. In case of “Unit 1” showing, press “Record” to start recording.
4. When the experiment is finished, push “Stop recording” button.
5. In some cases not all the data is sent in step 4. To be safe, in this step “Recollect” button should be pushed. This button sends the left over data from the sensor to the computer.
6. It is not necessary to press the “View data” button. This button shows each data string in a plot. It is possible to press this button while recording to see if the sensors are working correctly.
7. Press the “Write to file” button to write the experiment to the file. Pressing the button will create 9 text document files, the file names are made up with 16 numbers:
    - First 8 numbers are the date
        - Year first,
        - Then month and

    - At last the date
- Then there is a hyphen (-)
- The next 6 numbers are time of the day
    - First two is the hour (from 00 to 12)
    - Then the minutes (from 00 to 59)
    - Next the seconds (from 00 to 59)
- The last 2 numbers identify which sensor it is
    - The first 3 numbers (01,02,03) are the accelerometer
    - The next 3 numbers (04,05,06) are the gyroscope
    - The last 3 numbers (07,08,09) are the magnetometer

8. When the experiment is finished, press the "Exit" button.

3. Materials and Methods

3.1. Scaling and Examination of the IMU Data

The sensor writes out in nine different data files. Four experiments were executed to better understand what these data files represent and how the scale is. First three of these experiments were all carried out in the same way. The sensor was put on the table, then turned 90° around the one axis and 90° back, then the sensor was turned 180° around the same axis and 180° back. In the end the sensor was moved in the direction of that axis. In these three experiments, the x-, y- and z-axis where chosen respectively. The chosen coordinate system for the experiment can be seen in Figure 9.

For the fourth experiment the sensor was put on a table, and not moved for about 30 minutes. This was done to examine it the sensors would return the same results over longer period of time.

3.2. Recruitment of Subjects for the Experiment

To test the IMU sensor an experiment was performed on ten male athletes, who had given an informed consent for a biomechanical research. Reflective markers were placed on the subjects. The markers were placed on the fifth metatarsal, calcaneus, lateral malleolus, lateral tibial condyle, lateral femoral condyle and the hip. Additionally were two markers placed on the Kine IMU sensor. Weight of each individual was obtained by asking them about their last known weight.

3.3. Experimental Set-up

A camera, that was set to take a video with 300 frames/s, was on tripod perpendicular to a force plate, which was recording at 50 Hz. On either side of the force plate were four mats, two on each side, to enforce safety for the subjects. Two experiments were carried out on each subject, first the sensor, which was recording at 100 Hz, was placed on the subject's hip. For the second experiment the sensor was placed right above the knee of the dominant leg of the subject. An elastic belt was used to attach the sensor to each subject, this can be seen in Figures 9 and 15.

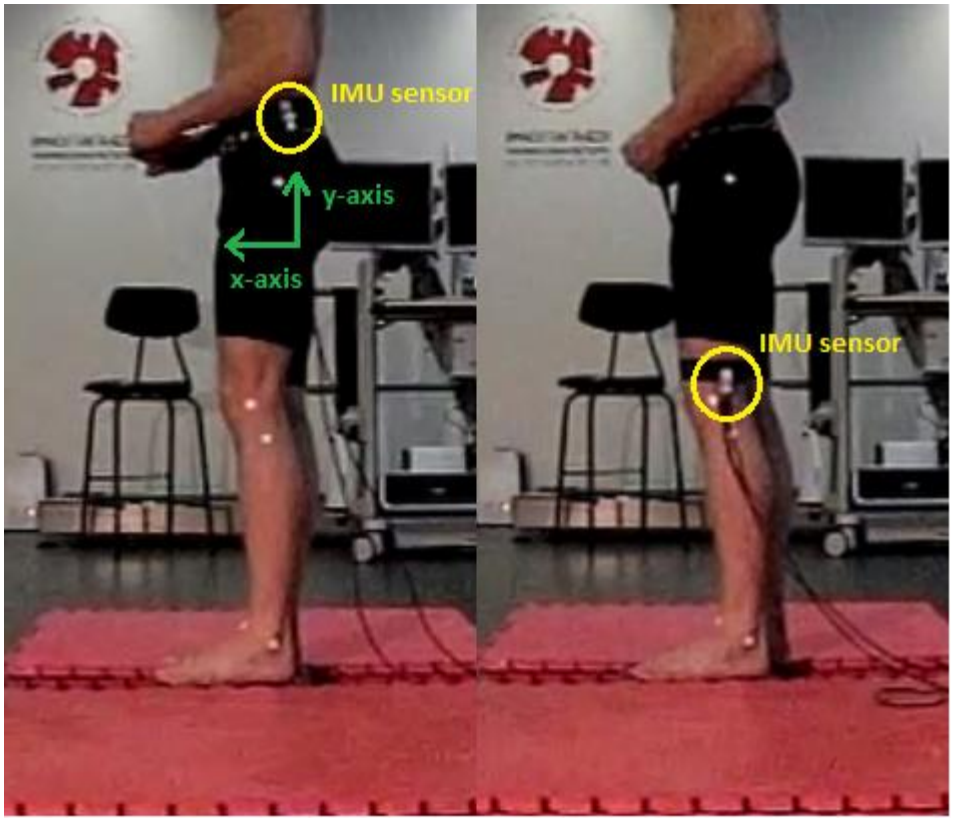

Figure 15: A picture from the experiment, to the left the IMU sensor is attached to the hip, to the right the IMU sensor is attached right above the knee

On Figure 15 the set-up of the experiment can be seen. To the left on the figure the Kine IMU sensor is attached to the hip, while to the right the sensor is attached right above the knee. Also in Figure 15 the coordinate system that is used in this experiment is shown (and can also be seen in Figure 9).

In the beginning of the experiment the subject would stand still, with his dominant leg perpendicular to the camera, on top of the force plate with the sensor attached to the hip on the

side that was turned to the camera. After starting recording on the camera, force plate and the Kine IMU sensor, the subject would start the experiment by tapping on the force plate with his dominant foot. The subject would jump straight up, as high as possible, while still landing safely on the force plate. After the subject would get his balance again and placed on the force plate, the jump was repeated. The first three subjects only jumped once. After that the camera, force plate and IMU sensor would be turned off, and the IMU sensor would be moved to the knee, facing the camera. Then the same process would start as described before.

3.4. Framework for Data Analysis Technique

Matlab was used for all signal processing. Collecting data from the video was started just before a movement was seen when the subject would tap on the force plate with his foot. Data cursor would be put on four markers on the subjects body, on the calcaneus, lateral malleolus, lateral tibial condyle and lateral femoral condyle, and on both of the markers on the Kine IMU sensor. This was done every 25 frames until the subject had landed and in an upright position after the second jump.

When comparing the data, from the Kine IMU sensor, force plate and the video data the open source IMU and AHRS algorithm by Sebastian Madgwick was used on the Kine IMU sensor data.

Before inserting the data from the Kine IMU sensor into the AHRS code some manipulation of the data had to be done. The acceleration data was represented as a multiply of the gravitational acceleration, g. The magnetometer data was represented in Gauss [G]. The gyroscope data was represented in degrees/sec which the data from the Kine IMU sensor generates its data in. The only other parameter that is put in the AHRS algorithm is the filter gain, β, which represents the divergent in each gyroscope.

4. Results

4.1. Scaling and Examination of the IMU Data

Figures 16 – 19 show the raw data from the Kine IMU sensor when carrying out scaling and examination of the data.

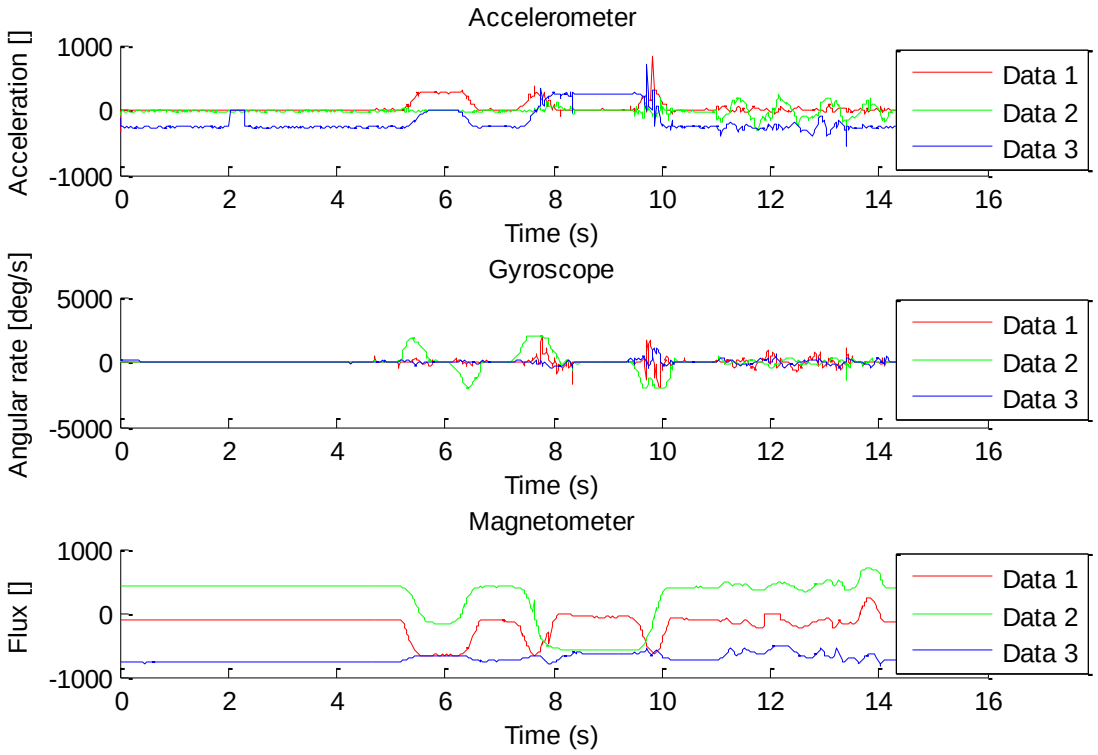

Figure 16: Turning the Kine IMU sensor around its x-axis

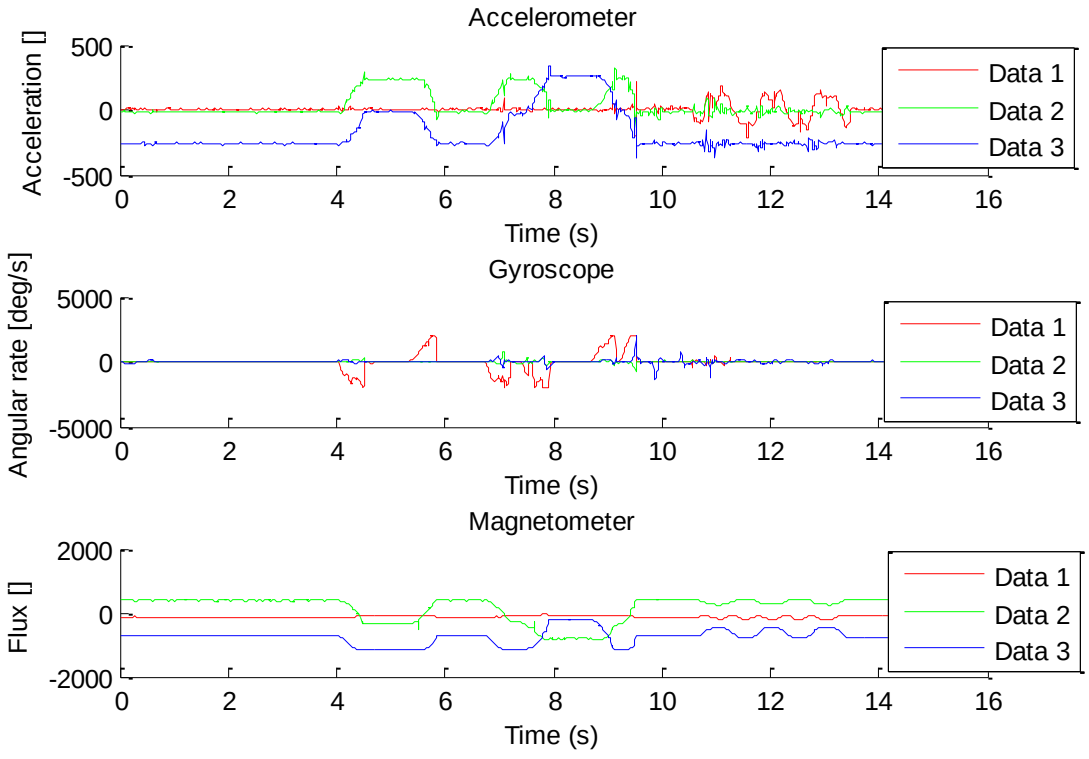

Figure 17: Turning the Kine IMU sensor around its y-axis

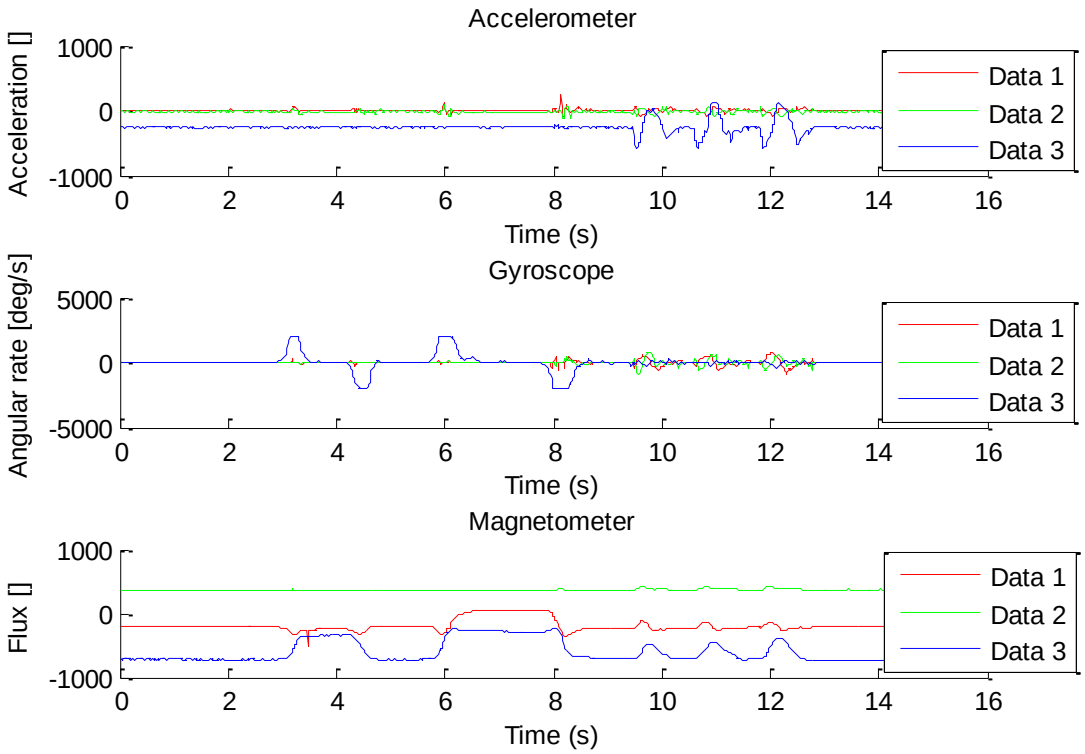

Figure 18: Turning the Kine IMU sensor around its z-axis

After examination of Figures 16-18 it can be seen that Data 1 correlates to movement around y-axis (Figure 17), Data 2 correlates to movement around x-axis (Figure 16) and Data 3 correlates to movement around z-axis (Figure 18). On each figure the gyroscope shows four distinct peaks that correlates to first moving the sensor 90° both ways, and then moving the sensor 180° front and back. Results from experimenting showed saturation of the angular velocity at 2048, which corresponded on average to 90°/0.4s angular velocity in the examination of the data in Figures 16-18. On the data from the accelerometer it can be seen after 10 to 11 sec on each figure what direction each sensor was sensing.

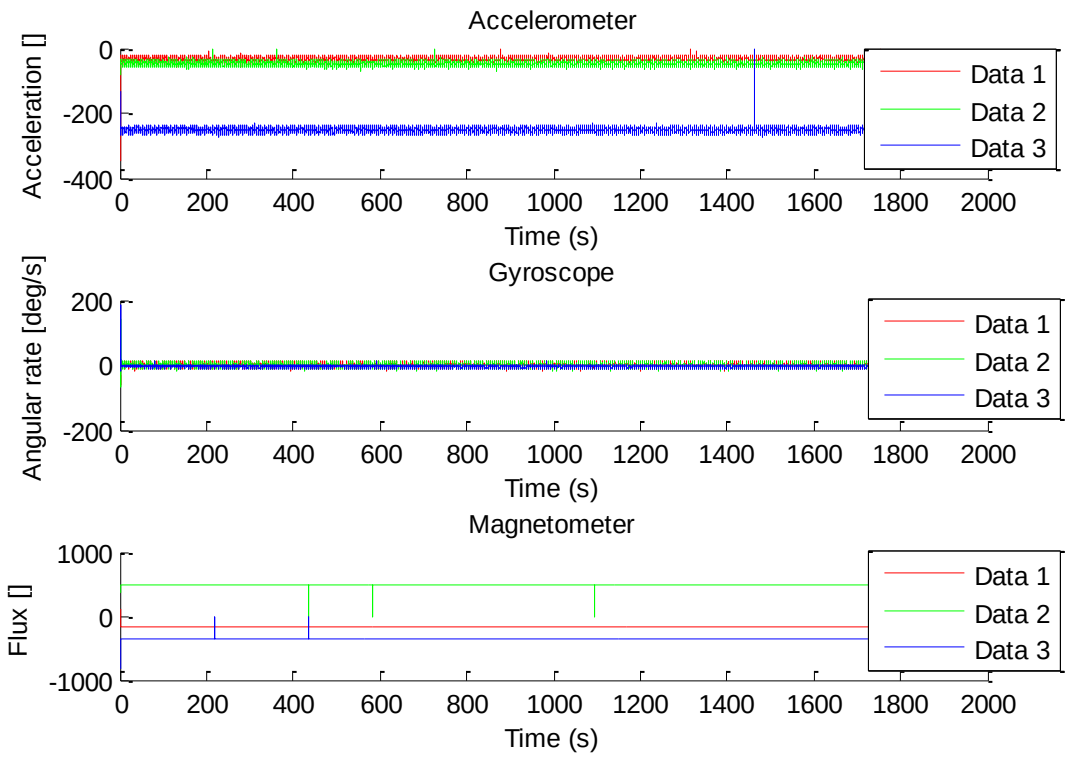

Figure 19: Kine IMU sensor lays still on table for about 30 minutes

In Figure 19 the Kine IMU sensor was put on a table, positioned so the z-axis was parallel to the earth and picked up the g-force. Average estimation of the sensor's output, representing the gravitational acceleration, g was -260±10, as can be seen in Figures 16-19. The sign before the signal represents the orientation of the sensor, if the sensor had been oriented 180° around z-axis the sign before the signal would have been opposite. On Figure 19 the data from accelerometer on x-, and y-axis was at -40, where the expected value would be 0, as it is on Figures 16-18, this indicates that sometimes there is an offset in the accelerometer data of about 40. From this information g was determined to be at 230. The earth's magnetic field at its surface is around 0.31-0.58 Gauss, from this knowledge it was decided to divide 1000 to the magnetometer data so the output from the magnetometer would be in that range. The divergent in the gyroscope is close to zero therefore the filter gain, β, was chosen at 0.1.

All sensor give a similar data over long period of time, except a few error spikes in the data from the magnetometer and accelerometer.

4.2. Biomechanical Experiment

Out of the 20 experiments that were done, two on each subject, twelve of the datasets were flawed in some way, in ten of them the gyroscope did not work properly (as seen in Figure 20) and in two of them the data from the force plate was faulty. In the end there were eight good datasets that were used to research. The eight datasets were from:

- Subject 1, sensor just above the knee
- Subject 3, sensor on the hip
- Subject 3, sensor just above the knee
- Subject 7, sensor on the hip
- Subject 8, sensor on the hip
- Subject 8, sensor just above the knee
- Subject 9, sensor on the hip
- Subject 9, sensor just above the knee

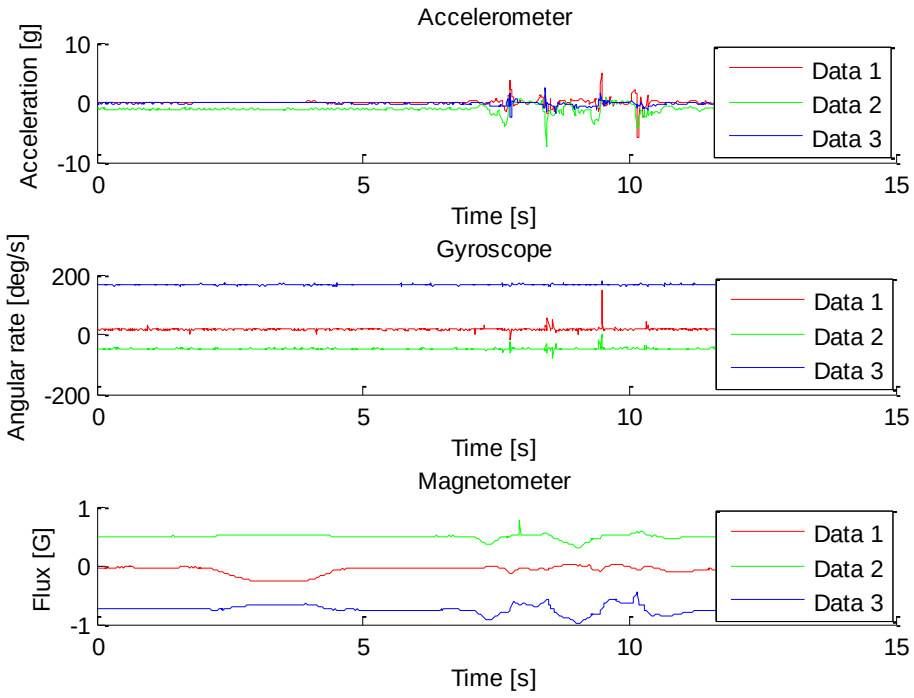

Figure 20: Subject 4, sensor on hip. It can be seen that the gyroscope is not working as it should

Figure 20 shows how the data looks from the gyroscope when it is not working properly.

The top image of Figures 21-28 show comparison, on each subject, of the y-axis dataset from the accelerometer in the Kine IMU sensor, the dataset from the force plate, and the dataset from the video analysis. The bottom image of the following Figures 21-28 show comparison, on each subject, of the angle change collected from the video analysis to the Euler corner for z-axis that the Matlab code created from information from the Kine IMU sensor.

Figure 21 shows an explanation of the peaks in the acceleration data from the experiment. The first peak represents the tap that the subject did. The next peak is the jump, at the same time as the acceleration increases an angle change happens since the subject start the jump by bending his knees and hip which creates an angle of the Kine IMU sensor. In between the jump peak and the landing peak the subject is in the air so no acceleration or angle change is occurring to the Kine IMU sensor as can be seen on the figure. The last peak on the figure represents the subject landing simultaneously there is an angle change since when the subject lands he bends the knees and hip which results in an angle change of the Kine IMU sensor.

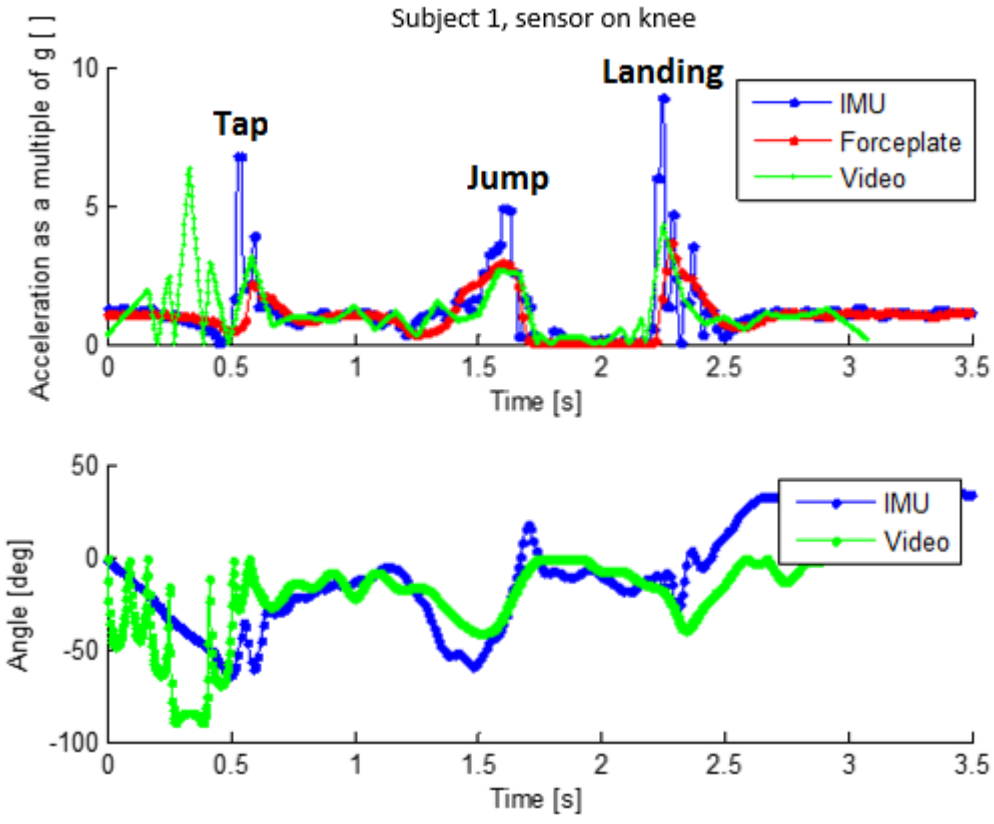

Figure 21: Comparison of different methods of measuring acceleration and angle of the Kine IMU sensor, on subject 1, where the sensor was put right above the knee

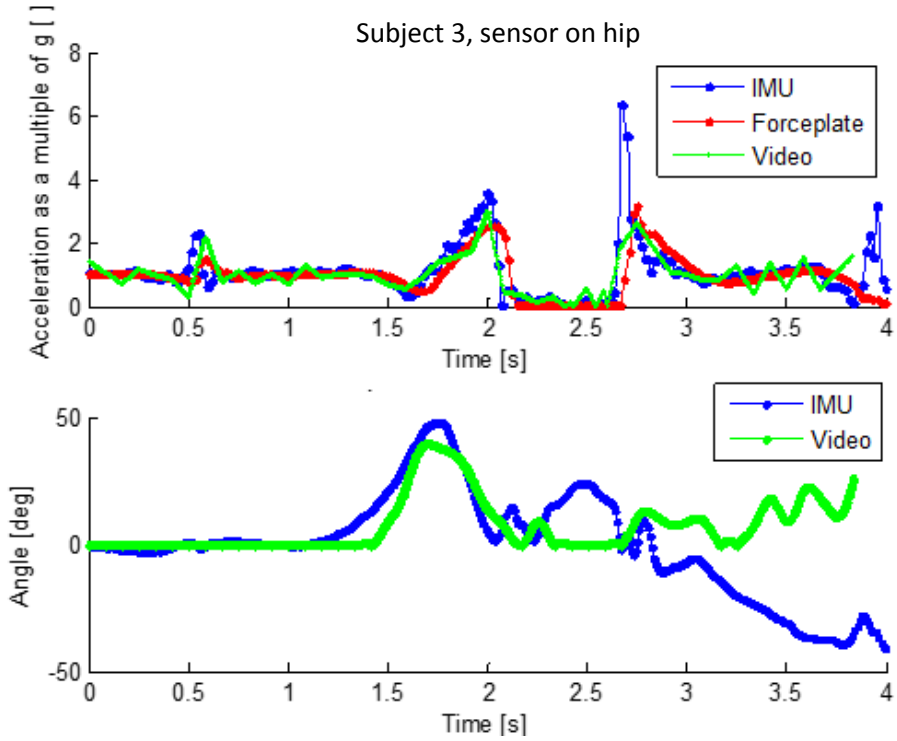

Figure 22: Comparison of different methods of measuring acceleration and angle of the Kine IMU sensor, on subject 3, where the sensor was put on the hip

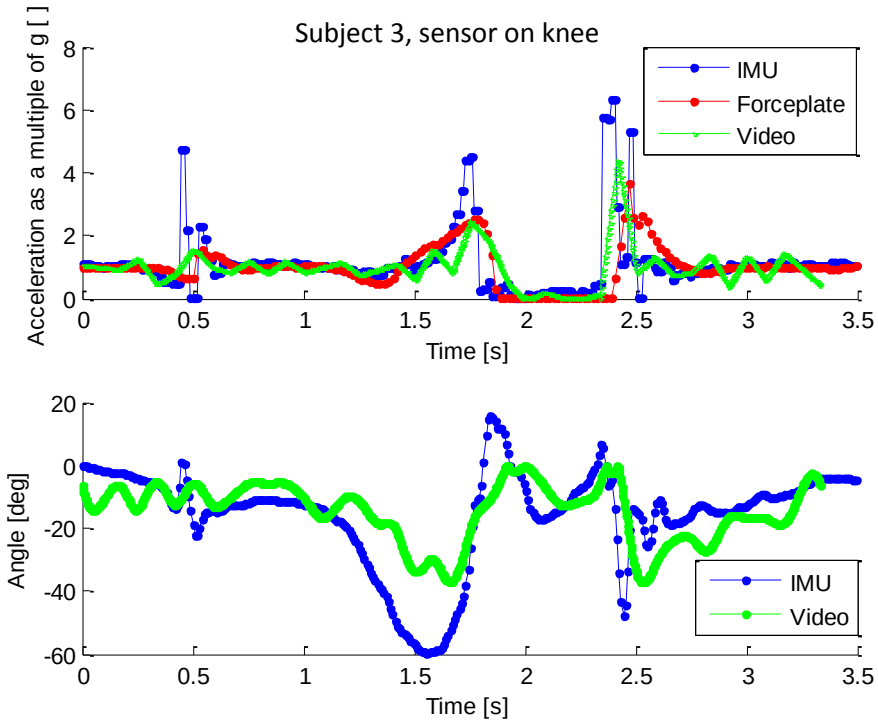

Figure 23: Comparison of different methods of measuring acceleration and angle of the Kine IMU sensor, on subject 3, where the sensor was put right above the knee

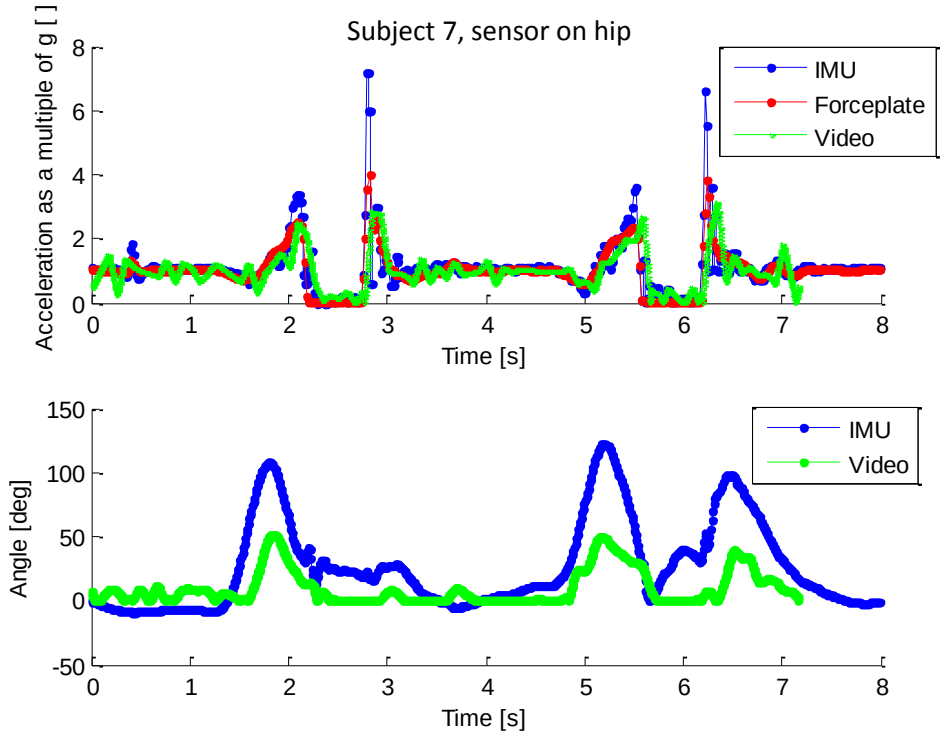

Figure 24: Comparison of different methods of measuring acceleration and angle of the Kine IMU sensor, on subject 7, where the sensor was put on the hip

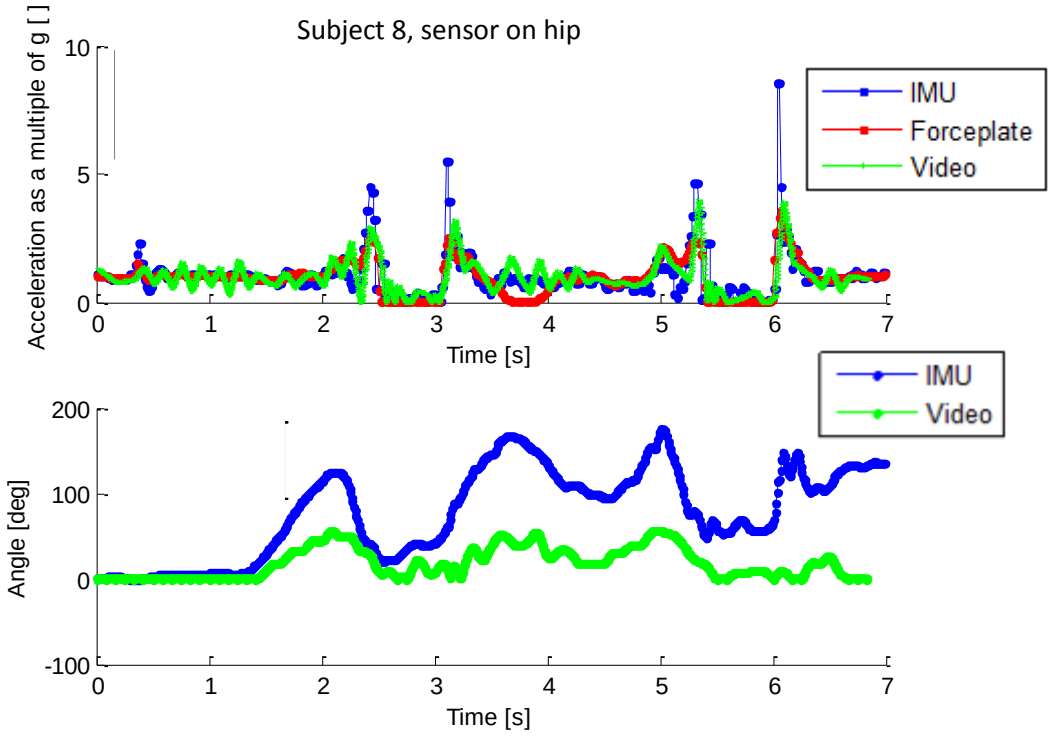

Figure 25: Comparison of different methods of measuring acceleration and angle of the Kine IMU sensor, on subject 8, where the sensor was put on the hip

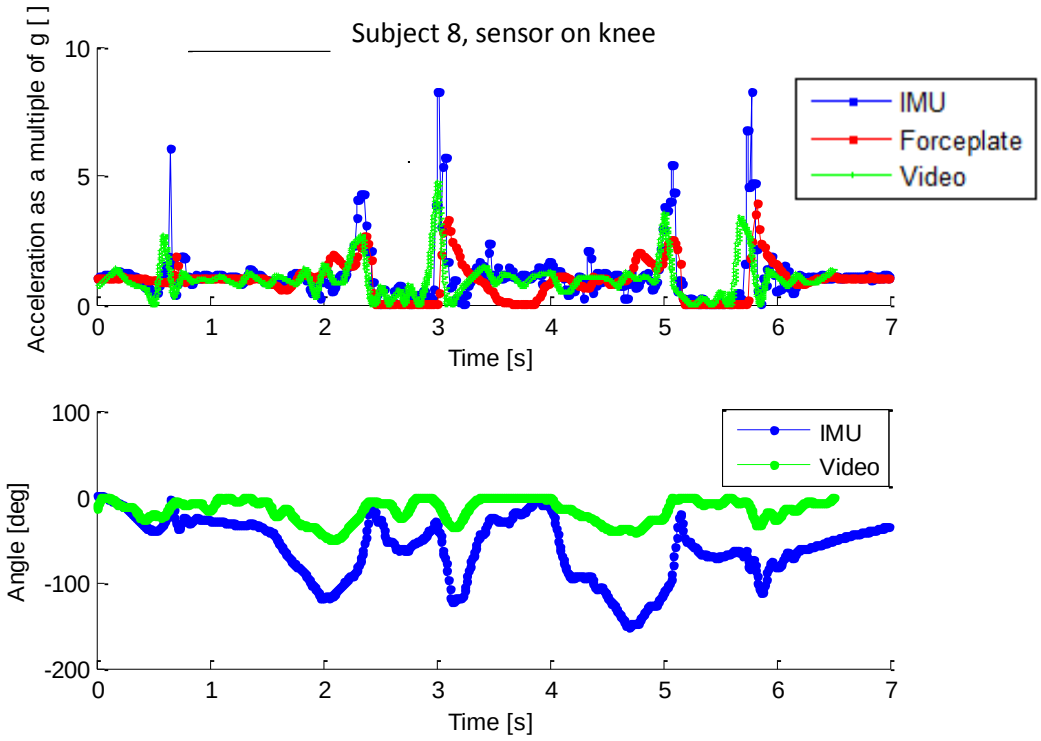

Figure 26: Comparison of different methods of measuring acceleration and angle of the Kine IMU sensor, on subject 8, where the sensor was put right above the knee

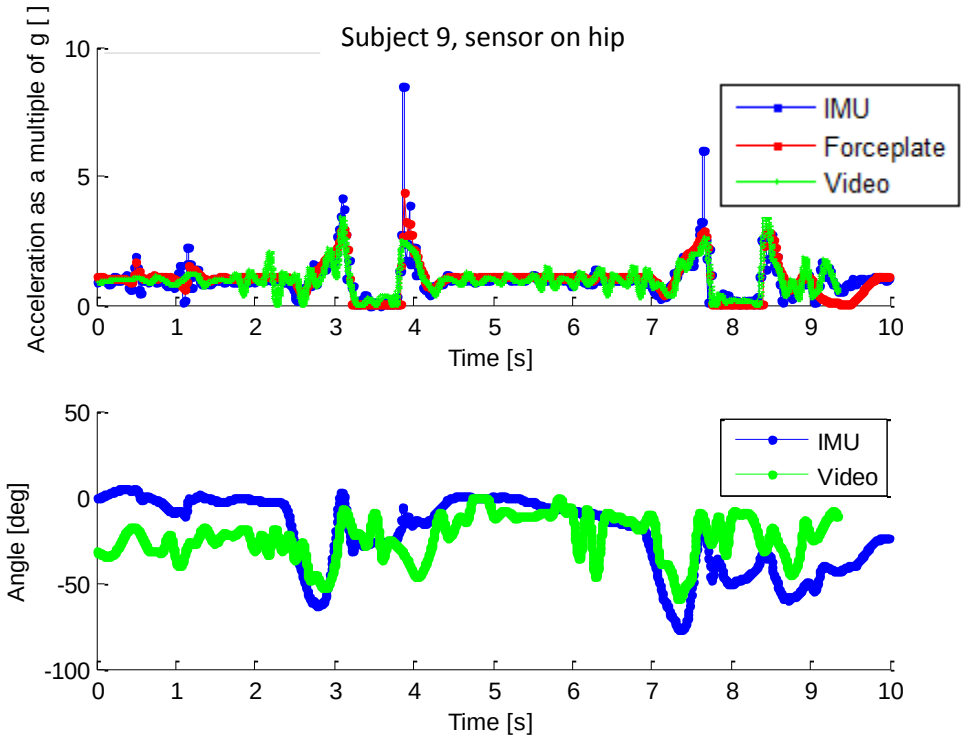

Figure 27: Comparison of different methods of measuring acceleration and angle of the Kine IMU sensor, on subject 9, where the sensor was put on the hip

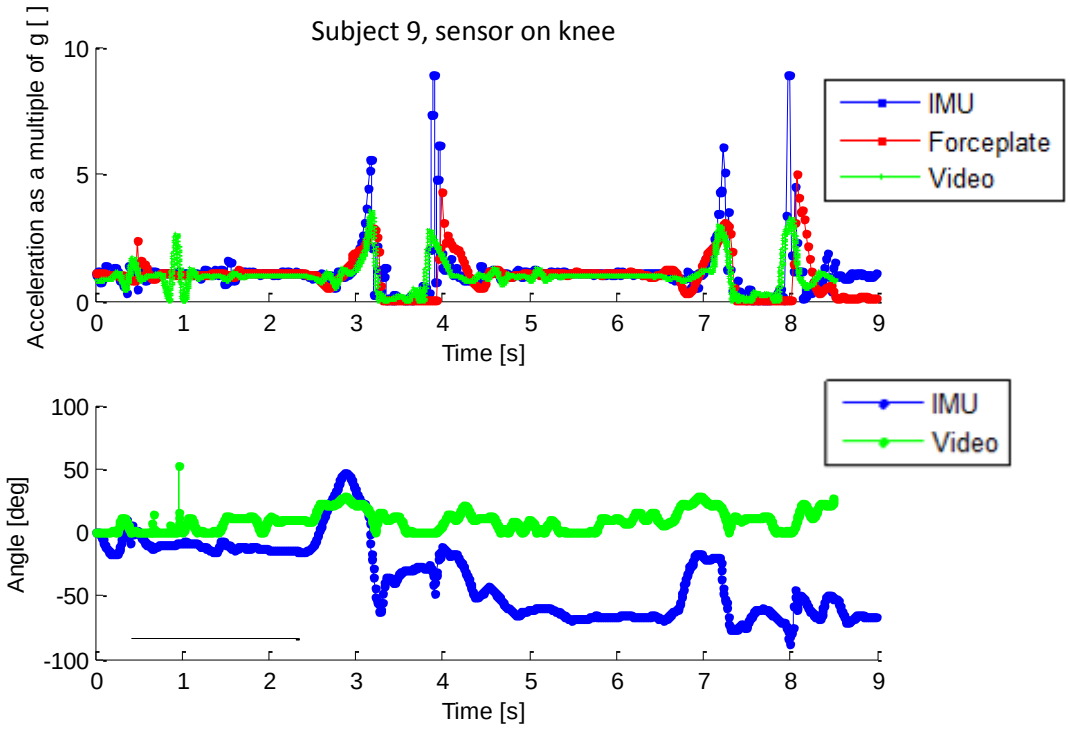

Figure 28: Comparison of different methods of measuring acceleration and angle of the Kine IMU sensor, on subject 9, where the sensor was put right above the knee

4.2.1. Other Data from the Experiment

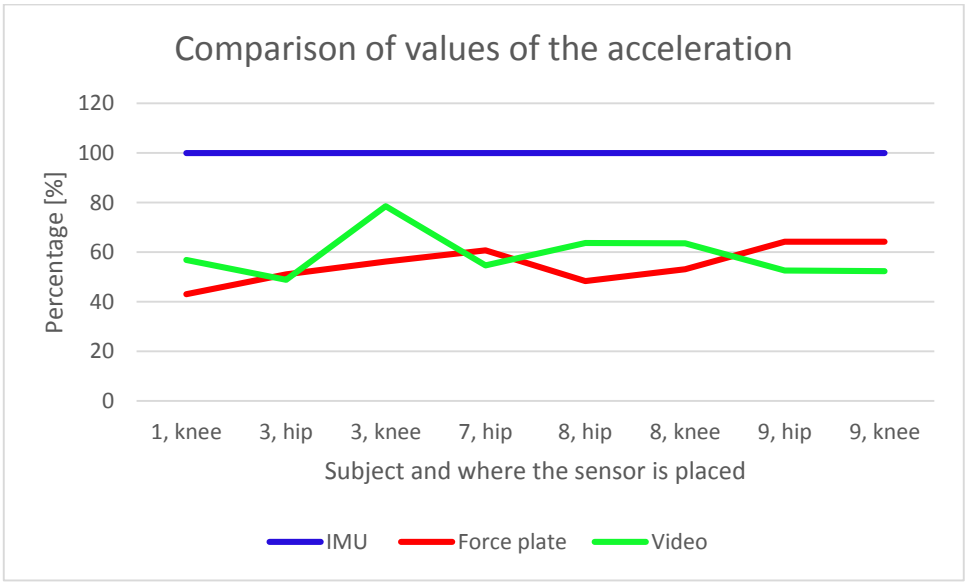

Figure 29: A comparison of the highest values of the acceleration data from the each subject

Figure 29 shows a comparison of the highest values, on each subject, on the acceleration data. The highest peaks were viewed, which happened just before and after the subject jumped.

Average difference between the highest peak (which was from data from the Kine IMU sensor in all experiments) to the peaks from the force plate and video were then calculated.

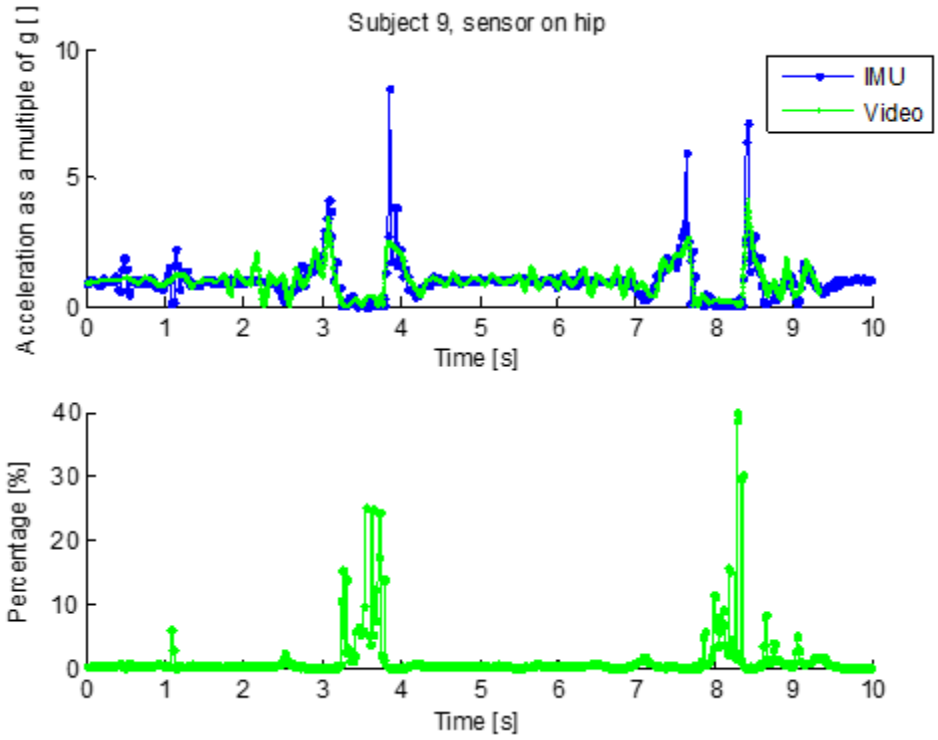

Figure 30: Percentage different between the data from the Kine IMU sensor to the video analysis. Dataset from subject 9, sensor on hip

Figure 30 shows in percentages how the datasets differs between the Kine IMU sensor and the video analysis. As can be seen in the figure the datasets are fairly similar except for the large peaks. From this it can be presumed that for slow acceleration the datasets are almost the same, but when there is a fast movement some errors between the datasets will occur.

Figure 31 shows all three Euler angles that AHRS code creates and the angle from the video analysis.

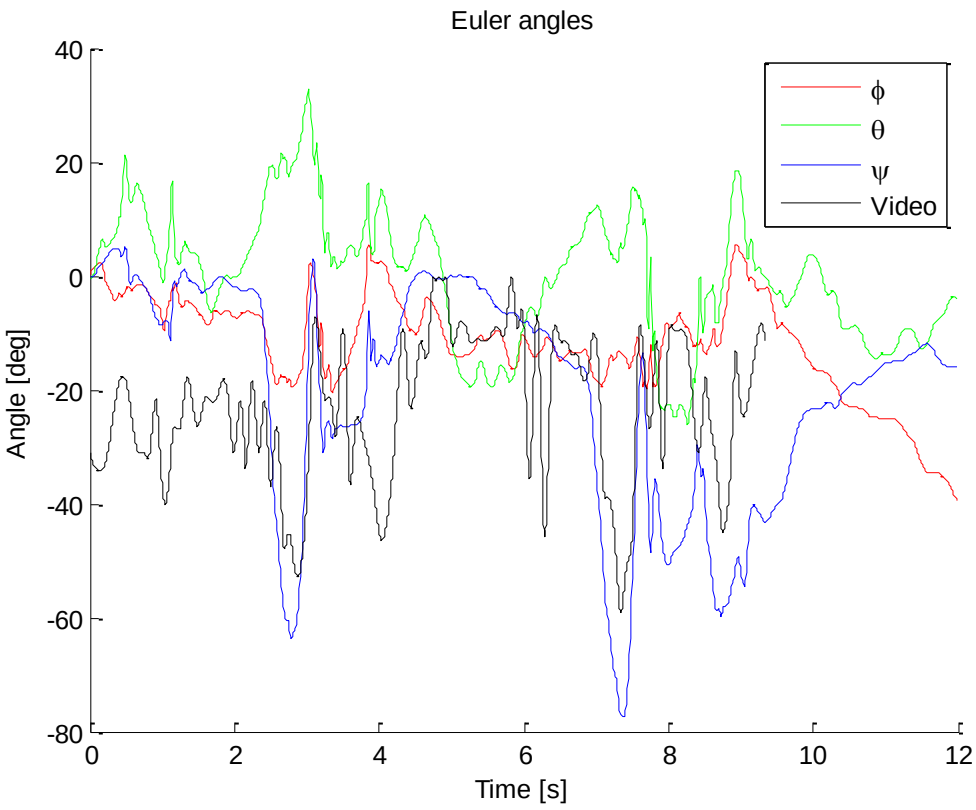

Figure 31: The Euler angles and the angle from the video analysis for subject 9, sensor on hip

In Figure 32 the movement of the Kine IMU sensor is captured by using the video analysis. In the figure the first jump has been categorized in four phases. First phase represents the subject standing still on the force plate. Next is the propulsion phase where the subject jumps up. After that is the flight phase where the subject is still in the air. The last phase is when the subject lands and gets his balance again.

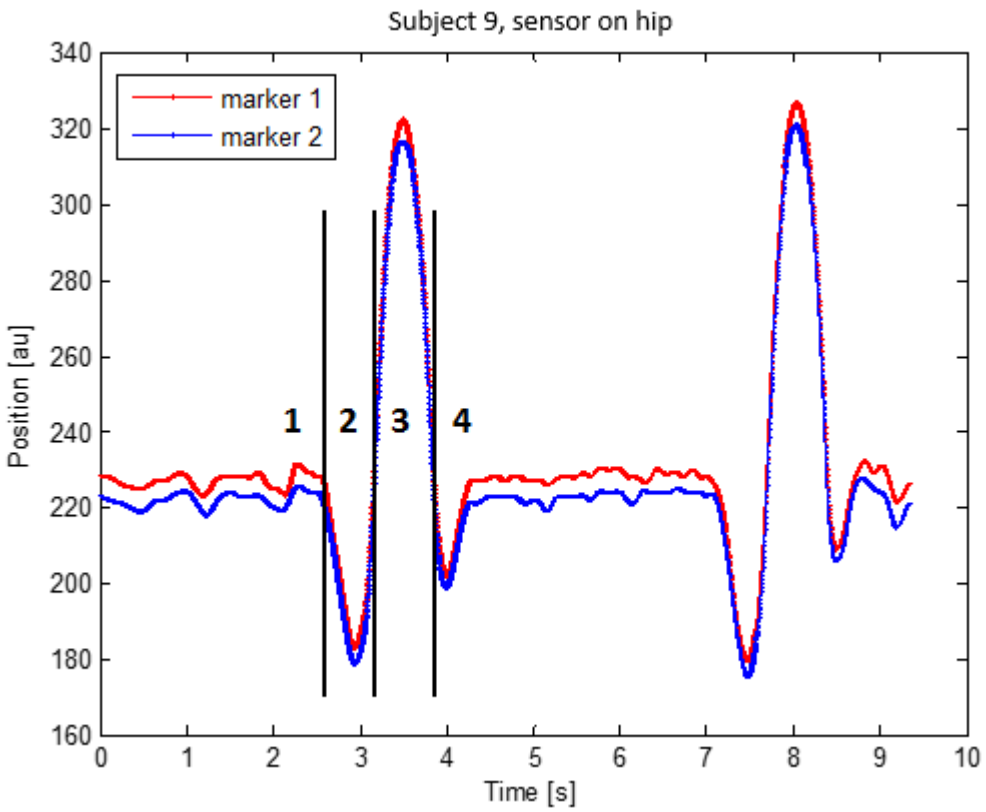

Figure 32: The movement of the Kine IMU sensor during the video analysis, on subject 9, sensor on hip

5. Discussions

5.1. The Experiment

The comparison of the acceleration data from the Kine IMU sensor, force plate, and video analysis, in chapter 4.2., shows that the accelerometer in the Kine IMU sensor is working properly. The tracks of the acceleration data are similar from all three measurement units, thought the peaks are always highest in the data from the Kine IMU sensor. The difference in amplitude of the peaks can be explained by the error in collecting the data, which is discussed in more details in chapter 5.2., another explanation is when the subjects lands he does not stop moving his knees or hip, rather he keeps on accelerating down which the force plate does not measure as accurately as the sensor does.

In the comparison of the angle calculated from the data from the Kine IMU sensor and the calculation from the video analysis, in chapter 4.2., it can be seen that the tracks of both

measurement units are similar. It is challenging to calculate the correct angle in the video analysis do to large errors in the video analysis data, as is described in chapter 5.2.2..

5.2. Errors Estimating

There are a few of factors that cause errors in the results.

5.2.1. Errors because of the Kine IMU Sensor

The USB cords that connect the Kine IMU sensor to the computer and power creates noise in the data from the sensor. Also these cords create added weight to the sensor and pull on it when the subject jumps, which inhibits the trajectory of the sensor.

The AHRS code calculates for the magnetometer as it is in the United Kingdom, there the vertical component due to the earth's magnetic field is at 65° to 70° to the horizontal axis [5]. In Iceland the earth's magnetic field is at about 78° to the horizontal axis [30].

The starting position of the accelerometer data, for when the sensor is still, varies by about 17%.

5.2.2. Errors because of the Video Analysis

Locating the data cursor in Matlab correctly on the marker on the Kine IMU sensor was challenging because of the resolution of the video. It resulted in large errors, especially in calculating the angle if the data cursor was not located correctly on the image.

Since the data was collected every 25th frame it is possible that some important data was missed, especially in fast movements like the landing.

5.2.3. Errors because of the Force Plate

The sampling frequency used in the force plate was 50 Hz, or half of what was used for the Kine IMU sensor. This could cause for the force plate to have missed some important data.

5.3. Future Work

5.3.1. Making the Connection from the Kine IMU to the Computer easier

It can be quite difficult to make a connection between the Kine IMU sensor and the computer

- If for some reason the KMUI2 test program is not closed in correct manner, for example if the program crashed for some reason or if the close button in the upper right corner is used to close the program, then it is a high possibility that the program did not close correctly and is still running in the background. To see if the program is still running, open task manager and search for the program. If is it present there, it is possible to close the program in the task manager window.
- Another connection problem can occur when connection the sensor to the computer, the computer can think that the sensor is a computer mouse and if that happens then the KMUI2 test program does not read the sensor. This can be avoided by turning off the Bluetooth in the computer.

5.3.2. Making the Sensor into one Unit

By having the sensor in two units some problems arise.

- The units are quite big, and the units need to be close together since the antenna only had a range of a few centimeters. In this research the units were taped together.
- It can be difficult to get a connection between the two units. It could not be trusted that by clicking on the "Record" button or "Stop record" in the KMIU2 test program, that measurement would start or stop. A double check always needs to be done to make sure that that either button has worked as it should. This is done by looking at the lights that are visible inside the measurement unit, when the unit is measuring the lights inside the measurement unit starts flashing more rapidly.

5.3.3. Making it Cordless

By not having the sensor cordless it limits the possibilities of usage of the sensor.

- The range of movement can only be as long as the cords, also the cords are quite big and voluminous and it can make a difference in how the subject would normally move.
- The cords also change the movement of the IMU sensor, due to the weight and stiffness of the cords the sensor does not move correctly with the movement of the subject.

5.3.4. Making the Sensor more Stable

It is of great importance that the three inner sensor work. In this experiment 20 subject experiments were carried out, two on each subject. Out of these 20 experiments only 10 of the Kine IMU data collected could be used because the gyroscope was not working properly. When working with the data after the experiments were finished it was easy to see that the gyroscope was dot collecting the data like it should, this can be seen on Figure 20, as the only movement on the gyroscope data can be associated to noise.

6. Conclusion

This Kine IMU sensor is well on its way on becoming the next generation sensor for Kine Measurement Unit. It is necessary to implement the recommendation of the changes and refinements which are discussed in chapter 5.3. before it is possible to use the Kine IMU sensor in research work or before selling them commercially. More research on this Kine IMU sensor still needs to be done for the few parameters that are changeable, like:

- Is it correctly assumed that the g-force is equal to 230 in the Kine IMU sensor?
- Is there a need of shifting the acceleration data to be sure it always has a starting point in zero?
- Is it correct to use 0.1 as the number for all mean zero gyroscope measurement errors (β)?
- Is there a need to change the data of the magnetometer because of the usage of the sensor in Iceland? If this sensor is going to be sold commercially all over the world, how is the program going to be able to change for every location?

References

[1] S. O. H. Madgwick, A. J. L. Harrison, and R. Vaidyanathan, "Estimation of IMU and MARG orientation using a gradient descent algorithm," in *2011 IEEE International Conference on Rehabilitation Robotics (ICORR)*, 2011, pp. 1–7.

[2] R. Zhu and Z. Zhou, "A real-time articulated human motion tracking using tri-axis inertial/magnetic sensors package," *IEEE Trans. Neural Syst. Rehabil. Eng.*, vol. 12, no. 2, pp. 295–302, Jun. 2004.

[3] S. Salehi, G. Bleser, N. Schmitz, and D. Stricker, "A Low-Cost and Light-Weight Motion Tracking Suit," in *Ubiquitous Intelligence and Computing, 2013 IEEE 10th International Conference on and 10th International Conference on Autonomic and Trusted Computing (UIC/ATC)*, 2013, pp. 474–479.

[4] D. T.-P. Fong and Y.-Y. Chan, "The Use of Wearable Inertial Motion Sensors in Human Lower Limb Biomechanics Studies: A Systematic Review," *Sensors*, vol. 10, no. 12, pp. 11556–11565, Dec. 2010.

[5] S. Madgwick, "An efficient orientation filter for inertial and inertial/magnetic sensor arrays.," Report x-io and University of Bristol (UK), 2010.

[6] N. A. A. Osman, F. Ibrahim, W. A. B. W. Abas, H. S. A. Rahman, and H. N. Ting, *4th Kuala Lumpur International Conference on Biomedical Engineering 2008: BIOMED 2008, 25-28 June 2008, Kuala Lumpur, Malaysia*. Springer, 2008.

[7] B. Þorgilsson, "Meeting about the IMU sensor," 23-Apr-2014.

[8] "KINE wireless surface electromyography (SEMG) & video for motion analysis in sports, research, science and rehabilitation | KMS (**K**ine **M**easurement **S**ystem)."[Online]. Available: http://kine.is/Products/MMS/. [Accessed: 07-May-2014].

[9] "About us." [Online]. Available: http://kine.is/About_us/. [Accessed: 08-May-2014].

[10] M. B. Popović, *Biomechanics and Robotics*. CRC Press, 2013.

[11] D. A. Winter, *Biomechanics and motor control of human movement*, 4th ed. Hoboken, N.J: Wiley, 2009.

[12] G. Robertson, G. Caldwell, J. Hamill, G. Kamen, and S. Whittlesey, *Research Methods in Biomechanics, 2E*. Human Kinetics, 2013.

[13] C. R. Ethier and C. A. Simmons, *Introductory Biomechanics: From Cells to Organisms*. Cambridge University Press, 2007.

[14] V. Choudhary and K. Iniewski, *MEMS: Fundamental Technology and Applications*. CRC Press, 2013.

[15] B. Siciliano and O. Khatib, *Springer Handbook of Robotics*. Springer, 2008.

[16] J. G. Webster and H. Eren, *Measurement, Instrumentation, and Sensors Handbook, Second Edition: Electromagnetic, Optical, Radiation, Chemical, and Biomedical Measurement*. CRC Press, 2014.

[17] P. Castillo, R. Lozano, and A. E. Dzul, *Modelling and Control of Mini-Flying Machines*. Springer, 2005.

[18] Y. Wu, *Advances in Computer, Communication, Control and Automation*. Springer, 2011.

[19] P. D. Groves, *Principles of GNSS, Inertial, and Multisensor Integrated Navigation Systems, Second Edition*. Artech House, 2013.

[20] P. Kim, *Kalman Filter for Beginners: With MATLAB Examples*. CreateSpace, 2011.

[21] J. B. Kuipers, *Quaternions and rotation sequences: a primer with applications to orbits, aerospace, and virtual reality*. Princeton, N.J.: Princeton University Press, 1999.

[22] "Open source IMU and AHRS algorithms | x-io Technologies." .

[23] S. Madgwick, *MadgwickAHRS.m*. 2011.

[24] K. J. O'Donovan, R. Kamnik, D. T. O'Keeffe, and G. M. Lyons, "An inertial and magnetic sensor based technique for joint angle measurement," *J. Biomech.*, vol. 40, no. 12, pp. 2604–2611, 2007.

[25] R. E. Mayagoitia, A. V. Nene, and P. H. Veltink, "Accelerometer and rate gyroscope measurement of kinematics: an inexpensive alternative to optical motion analysis systems," *J. Biomech.*, vol. 35, no. 4, pp. 537–542, Apr. 2002.

[26] M. C. Boonstra, R. M. A. van der Slikke, N. L. W. Keijsers, R. C. van Lummel, M. C. de Waal Malefijt, and N. Verdonschot, "The accuracy of measuring the kinematics of rising from a chair with accelerometers and gyroscopes," *J. Biomech.*, vol. 39, no. 2, pp. 354–358, Jan. 2006.

[27] D. Roetenberg, P. J. Slycke, and P. H. Veltink, "Ambulatory Position and Orientation Tracking Fusing Magnetic and Inertial Sensing," *IEEE Trans. Biomed. Eng.*, vol. 54, no. 5, pp. 883–890, May 2007.

[28] STMicroelectronics, "MEMS motion sensor: ultra-stable three-axis digital output gyroscope," 17116, Dec. 2010.

[29] STMicroelectronics, "Sensor module: 3-axis accelerometer and 3-axis magnetometer," 16941, Dec. 2009.

[30] W. G. V.-M. P. members International Association of Geomagnetism and Aeronomy, C. C. Finlay, S. Maus, C. D. Beggan, T. N. Bondar, A. Chambodut, T. A. Chernova, A. Chulliat, V. P. Golovkov, B. Hamilton, M. Hamoudi, R. Holme, G. Hulot, W. Kuang, B. Langlais, V. Lesur, F. J. Lowes, H. Lühr, S. Macmillan, M. Mandea, S. McLean, C. Manoj, M. Menvielle, I. Michaelis, N. Olsen, J. Rauberg, M. Rother, T. J. Sabaka, A. Tangborn, L. Tøffner-Clausen, E. Thébault, A. W. P. Thomson, I. Wardinski, Z. Wei, and T. I. Zvereva, "International Geomagnetic Reference Field: the eleventh generation," *Geophys. J. Int.*, vol. 183, no. 3, pp. 1216–1230, Dec. 2010.

Appendix A - Matlab Code

```
%Choose the video file
[file_name_mat, path_name_mat] = uigetfile('*.mat','Choose a video file')
load(strcat(path_name_mat,'\',file_name_mat));

%Double differentiation for location
for i=1:6
    jj=0;
    for j=2:length(XX)-1
        jj=jj+1;
        dXdt(jj,i)=(XX(j-1,i)-XX(j+1,i))/(2*dt(1));
        ddXdt(jj,i)=(XX(j-1,i)-2*XX(j,i)+XX(j+1,i))/(dt(1)^2);
        dYdt(jj,i)=(YY(j-1,i)-YY(j+1,i))/(2*dt(1));
        ddYdt(jj,i)=(YY(j-1,i)-2*YY(j,i)+YY(j+1,i))/(dt(1)^2);
    end
end

ay=abs((ddYdt+2000)/2000);
ax=abs((ddXdt+2000)/2000);

%Choose the IMU data
[file_name, path_name] = uigetfile('*.txt','Choose the first IMU data file')
X(:,1)=load(file_name);
N=length(X);

for i = 2:9
    next_file=strcat(file_name(1:end-5),num2str(i),'.txt');
    X_dummy=load(next_file);
    N_dummy=length(X_dummy);
    if N_dummy==N
        X(:,i)=X_dummy;
    elseif N_dummy<N
        X(:,i)=zeros(N,1);
        X(1:N_dummy)=X_dummy;
    elseif N_dummy>N
        X(:,i)=X_dummy(1:N);
    end
end

f=100;
T = N/f;
t_imu=linspace(0,T,N);
t_imu=t_imu';
 g=230; %Number chosen for g

%Choose force plate file
[file_name_force, path_name_force] = uigetfile('*.txt','Choose force plate
file')
K=load(strcat(path_name_force,'\',file_name_force));
Thyngd = input('What is the weight of the subject? ');

t_f=K(:,1);
t_f=t_f-t_f(1);
F=K(:,2);
```

```
figure
plot(t_imu,abs(X(:,1)/g),'b.-')
hold
plot(t_f,F/(Thyngd*9.82),'r.-')
plot(timi_fine(2:end-1),ay(:,1),'g+-','markersize',2);
xlabel('Time [s]');
ylabel('Acceleration as a multiple of g [ ]')
legend('IMU', 'Forceplate','Video')

%Choose the same event for all the data to configure the data
h = datacursormode;
datacursormode on
pause
s = getCursorInfo(h);

t0_imu=s(1).Position(1)-s(3).Position(1);
t0_f=s(2).Position(1)-s(3).Position(1);

StartIMU = round(abs(t0_imu)*100);
StartKraft = round(abs(t0_f)*50);

%Changing the start point for data from the IMU sensor
NN=N-StartIMU+1;
for i=1:9
    XIMU(:,i)=zeros(NN,1);
    XIMU(:,i)=X(StartIMU:end,i);
End

f=100;
TIMU = NN/f;
t_ximu=linspace(0,TIMU,NN);
t_ximu=t_ximu';
time=t_ximu;

%Changing the start point for data from the force plate
NK=length(K);
NNK=NK-StartKraft+1;
KK(:,2)=zeros(NNK,1);
KK(:,2)=K(StartKraft:end,2);
F=KK(:,2);

fK=50;
TK = NNK/fK;
t_kf=linspace(0,TK,NNK);
t_kf=t_kf';

%Changing the data to correct format to fit in the AHRS code
A1=(XIMU(:,1)/g);
A2=(XIMU(:,2)/g);
A3=(XIMU(:,3)/g);
G1=XIMU(:,4);
G2=XIMU(:,5);
G3=XIMU(:,6);
M1=(XIMU(:,7))/1000;
M2=(XIMU(:,8))/1000;
M3=(XIMU(:,9))/1000;
```

```
Accelerometer = [[A2] [A1] [A3]];
Gyroscope = [[G2] [G1] [G3]];
Magnetometer = [[M2] [M1] [M3]];
FF=F/(Thyngd*9.82);

Lengd_ximu=100*12; %How long should the figure be in seconds, IMU data
Lengd_kf = 50*12; %How long should the figure be in seconds, force plate data

%adapted AHRS code for this experiment
addpath('quaternion_library');

figure('Name', 'Subject 9, sensor on hip');
axis(1) = subplot(3,1,1);
hold on;
plot(time(1:Lengd_ximu), Gyroscope(1:Lengd_ximu,1), 'r');
plot(time(1:Lengd_ximu), Gyroscope(1:Lengd_ximu,2), 'g');
plot(time(1:Lengd_ximu), Gyroscope(1:Lengd_ximu,3), 'b');
legend('X', 'Y', 'Z');
xlabel('Time (s)');
ylabel('Angular rate (deg/s)');
title('Gyroscope');
hold off;
axis(2) = subplot(3,1,2);
hold on;
plot(time(1:Lengd_ximu), Accelerometer(1:Lengd_ximu,1), 'r');
plot(time(1:Lengd_ximu), Accelerometer(1:Lengd_ximu,2), 'g');
plot(time(1:Lengd_ximu), Accelerometer(1:Lengd_ximu,3), 'b');
legend('X', 'Y', 'Z');
xlabel('Time (s)');
ylabel('Acceleration (g)');
title('Accelerometer');
hold off;
axis(3) = subplot(3,1,3);
hold on;
plot(time(1:Lengd_ximu), Magnetometer(1:Lengd_ximu,1), 'r');
plot(time(1:Lengd_ximu), Magnetometer(1:Lengd_ximu,2), 'g');
plot(time(1:Lengd_ximu), Magnetometer(1:Lengd_ximu,3), 'b');
legend('X', 'Y', 'Z');
xlabel('Time (s)');
ylabel('Flux (G)');
title('Magnetometer');
hold off;
linkaxes(axis, 'x');

AHRS = MadgwickAHRS('SamplePeriod', 1/256, 'Beta', 0.1);

quaternion = zeros(length(time), 4);
for t = 1:length(time)
    AHRS.Update(Gyroscope(t,:)      *      (pi/180),      Accelerometer(t,:),
Magnetometer(t,:));  % gyroscope units must be radians
    quaternion(t, :) = AHRS.Quaternion;
end
```

```
euler = quatern2euler(quaternConj(quaternion)) * (180/pi);  % use conjugate for
sensor frame relative to Earth and convert to degrees.

figure('Name', 'Euler Angles and calculated');
hold on;
plot(time(1:Lengd_ximu), euler(1:Lengd_ximu,1), 'r');
plot(time(1:Lengd_ximu), euler(1:Lengd_ximu,2), 'g');
plot(time(1:Lengd_ximu), euler(1:Lengd_ximu,3), 'b');
plot(timi_fine,(abs(phi)-90),'k')
title('Euler angles');
xlabel('Time [s]');
ylabel('Angle [deg]');
legend('\phi', '\theta', '\psi', 'Video');
hold off;


figure
plot(t_ximu(1:Lengd_ximu),abs(XIMU(1:Lengd_ximu,1)/g),'b.-')
hold
plot(t_kf(1:Lengd_kf),FF(1:Lengd_kf,1),'r.-')
plot(timi_fine(2:end-1),abs((ddYdt+2000)/2000),'g-','markersize',2);
title('Subject 1, sensor on knee')
xlabel('Time [s]');
ylabel('Acceleration as a multiple of g [ ]')
legend('IMU', 'Forceplate','Video')


figure('Name', 'Sensor Data');
axis(1) = subplot(2,1,1);
hold on;
plot(t_ximu(1:Lengd_ximu),abs(XIMU(1:Lengd_ximu,1)/g),'b.-')
plot(t_kf(1:Lengd_kf),FF(1:Lengd_kf,1),'r.-')
plot(timi_fine(2:end-1),abs((ddYdt(:,1)+2000)/2000),'g+-','markersize',2);
xlabel('Time [s]');
ylabel('Acceleration as a multiple of g [ ]')
legend('IMU', 'Forceplate','Video')
title('Subject 9, sensor on knee')
hold off;
axis(2) = subplot(2,1,2);
hold on;
plot(time(1:Lengd_ximu), euler(1:Lengd_ximu,3), 'b.-');
plot(timi_fine,abs(abs(phi)-90),'g.-')
xlabel('Time [s]');
ylabel('Angle [deg]');
legend('IMU','Video');
hold off;
```